A test of an optimal stomatal conductance scheme within the CABLE Land Surface Model

M. G. De Kauwe[1], J. Kala[2], Y.-S. Lin[1], A. J. Pitman[2], B. E. Medlyn[1], R. A. Duursma[3], G. Abramowitz[2], Y.-P. Wang[4] and D. G. Miralles[5,6]

[1]{Macquarie University, Sydney, Australia}

[2]{Australian Research Council Centre of Excellence for Climate Systems Science and Climate Change Research Centre}

[3]{Hawkesbury Institute for the Environment, University of Western Sydney, Sydney, Australia}

[4]{CSIRO Ocean and Atmosphere Flagship, Private Bag #1, Aspendale, Victoria 3195, Australia}

[5]{Department of Earth Sciences, VU University, Amsterdam 1081 HV, The Netherlands}

[6]{Laboratory of Hydrology and Water Management, Ghent University, B-9000 Ghent, Belgium}

Correspondence to: M. G. De Kauwe (mdekauwe@gmail.com)

Abstract

Stomatal conductance (g_s) affects the fluxes of carbon, energy and water between the vegetated land surface and the atmosphere. We test an implementation of an optimal stomatal conductance model within the Community Atmosphere Biosphere Land Exchange (CABLE) land surface model (LSM). In common with many LSMs, CABLE does not differentiate between g_s model parameters in relation to plant functional type (PFT), but instead only in relation to photosynthetic pathway. We constrained the key model parameter "g_1", which represents plant water use strategy, by PFT, based on a global synthesis of stomatal behaviour. As proof of concept, we also demonstrate that the g_1 parameter can be estimated using two long-term average (1960-1990) bioclimatic variables: (i) temperature and (ii) an indirect estimate of annual plant water availability. The new stomatal model, in conjunction

with PFT parameterisations, resulted in a large reduction in annual fluxes of transpiration (~30 % compared to the standard CABLE simulations) across evergreen needleleaf, tundra and C4 grass regions. Differences in other regions of the globe were typically small. Model performance against upscaled data products was not degraded, but did not noticeably reduce existing model-data biases. We identified assumptions relating to the coupling of the vegetation to the atmosphere and the parameterisation of the minimum stomatal conductance as areas requiring further investigation in both CABLE and potentially other LSMs. We conclude that optimisation theory can yield a simple and tractable approach to predicting stomatal conductance in LSMs.

1 Introduction

Land surface models (LSMs) provide the lower boundary conditions for the atmospheric component of global climate and weather prediction models. A key role for LSMs is to calculate net radiation available at the surface and its partitioning between sensible and latent heat fluxes (Pitman, 2003). To achieve this, LSMs calculate latent heat exchange between the soil, vegetation and the atmosphere. This latent heat exchange involves a transfer of water vapour to the atmosphere; for vegetated surfaces this transfer (i.e. transpiration) occurs mostly through the stomatal cells on the leaves as they open to uptake CO_2 for photosynthesis, but also includes interception losses from the canopy. Transpiration from the vegetation has been estimated to account for 60-80% of evapotranspiration (ET) across the land surface (e.g., Miralles et al. 2011; Jasechko et al. 2013; Schlesinger and Jasechko, 2014, but see Schlaepfer et al. 2014). The stomata are thus the principal control over the exchange of water and the associated flux of carbon dioxide (CO_2) between the leaf and the atmosphere. Stomatal conductance (g_s) plays a significant role in the global carbon, energy and water cycles, hence it modulates climate feedbacks and plays a critical role in global change (Henderson-Sellers et al., 1995; Pollard and Thompson, 1995; Cruz et al., 2010; Sellers et al. 1996; Gedney et al. 2006; Betts et al. 2007; Cao et al. 2010).

In both ecosystem and land surface models, it is common to represent g_s with empirical models (Jarvis, 1976; Ball et al. 1987; Leuning, 1995; see Damour et al. 2010 for a review). In a recent inter-comparison study, 10 of the 11 ecosystem models considered applied some form of the "Ball-Berry-Leuning" approach (De Kauwe et al. 2013a). The empirical nature of these models means that we cannot attach any theoretical significance to differences in model parameters across datasets or among species. As a consequence, models which use these schemes commonly either assume the model parameters only vary with photosynthetic pathway, or tune the parameters to match a specific experiment where necessary. Whilst more mechanistic g_s models have been proposed (e.g. Buckley et al. 2003; Wang et al. 2012), they have not been widely applied due to their relative complexity and the need to obtain additional model parameters, for which we have no (or limited) observational data across a variety of PFTs.

An alternative approach, originally proposed by Cowan and Farquhar (1977) and Cowan (1982), is to model stomatal conductance using an optimisation framework (Hari et al. 1986; Lloyd, 1991; Arneth et al. 2002; Katul et al. 2009; Schymanski et al. 2009; Medlyn et al. 2011). This approach hypothesises that optimal stomatal behaviour occurs when the carbon gain (photosynthesis, A) is maximised, whilst minimising water loss (transpiration, E) over some period of time (t_2-t_1). Therefore, optimal stomatal behaviour is the result of maximising:

$$\int_{t_1}^{t_2} \left(A(t) - \lambda E(t)\right) dt \quad (1)$$

where λ (mol^{-1} C mol^{-1} H_2O) is the marginal carbon cost of water use.

Medlyn et al. (2011) recently proposed a tractable model that analytically solves the optimisation problem. This model has great potential because it combines a simple functional form, similar to current empirical approaches, with a theoretical basis. Biological meaning can be attached to the parameters, which can then be hypothesised to vary with climate and plant water use strategy (Medlyn et al. 2011; Héroult et al. 2013; Lin et al. 2015). In addition, the behaviour of this model has been widely tested at the leaf scale and it has been shown to perform at least as well, if not better than, the more widespread empirical approaches currently used (Medlyn et al. 2011; De Kauwe et al. 2013a; Duursma et al. 2013; Medlyn et al. 2013; Héroult et al. 2013). We also note that it is possible to implement a numerical solution of this optimisation problem into a LSM (Bonan et al. 2014).

Here, we present an implementation of the Medlyn et al. (2011) optimal stomatal conductance model within the Community Atmosphere Biosphere Land Exchange (CABLE) LSM (Wang et al. 2011). CABLE is the LSM used within the Australian Community Climate Earth System Simulator (ACCESS, see http://www.accessimulator.org.au; Kowalczyk et al. 2013), a fully coupled earth system model used as part of the Coupled Model Intercomparison Project (CMIP-5), which in turn informed much of the climate projection research underpinning the 5th assessment report of the Intergovernmental Panel on Climate Change. CABLE currently implements an empirical representation of g_s following Leuning et al. (1995). The existing CABLE parameterisation of stomatal conductance, similar to other

LSMs, including the Community Land Model version 4.5 (CLM4.5: Oleson et al. 2013) and the ORganizing Carbon and Hydrology in Dynamic EcosystEms model (ORCHIDEE: Krinner et al. 2005), only characterises differences in stomatal behaviour relating to photosynthetic pathway, rather than PFT. The implementation assumes that all PFTs can be adequately described by three parameters, two of which vary with photosynthetic pathway. Simulated latent heat (LE) by CABLE has been shown to be sensitive to these parameters (Lu et al. 2013), but the origin of this parameterisation has not been well documented in the literature. In contrast, here we seek to constrain the new Medlyn model implementation with data derived from a recent global synthesis of stomatal behaviour (Lin et al. in 2015). We first test the implementation of the new g_s scheme at a series of flux tower sites and then undertake a series of offline simulations to examine the model's behaviour at the global scale.

2 Methods

2.1 Model description

The CABLE LSM has been used extensively for both coupled (Cruz et al. 2010; Pitman et al. 2011; Mao et al. 2011; Lorenz et al. 2014) and offline simulations (Abramowitz et al. 2008; Wang et al. 2011; Kala et al. 2014) at a range of spatial scales. CABLE represents the canopy using a single layer, two-leaf canopy model separated into sunlit and shaded leaves (Wang and Leuning, 1998), with aerodynamic properties simulated as a function of canopy height and leaf area index (LAI) (Raupach 1994; Raupach et al. 1997). The Richards' equation for soil water and heat conduction is numerically integrated using six discrete soil layers, and up to three layers of snow can accumulate on the soil surface. A complete description can be found in Kowalczyk et al. (2006) and Wang et al. (2011). The source code can be accessed after registration at https://trac.nci.org.au/trac/cable.

2.2 Stomatal model and parameterisation.

In CABLE, g_s (stomatal conductance, mol m^{-2} s^{-1}) is modelled following Leuning (1995):

$$g_s = g_0 + \frac{a_1 \beta A}{(C_s - \Gamma)\left(1 + \frac{D}{D_0}\right)} \quad (2)$$

where A is the net assimilation rate (μmol m^{-2} s^{-1}), C_s (μmol mol^{-1}) and D (kPa) are the CO_2 concentration and the vapour pressure deficit at the leaf surface, respectively, Γ (μmol mol^{-1}) is the CO_2 compensation point of photosynthesis, and g_0 (mol m^{-2} s^{-1}), D_0 (kPa) and a_1 are fitted constants representing the residual stomatal conductance as net assimilation rate reaches zero, the sensitivity of stomatal conductance to D and the slope of the sensitivity of stomatal conductance to assimilation, respectively. In CABLE, the fitted parameters g_0 and a_1 vary with photosynthetic pathway (C3 vs C4) but not PFT, and D_0 is fixed for each PFTs. g_0 is scaled from the leaf to the canopy by accounting for LAI, following Wang and Leuning (1998). β represents an empirical soil moisture stress factor:

$$\beta = \frac{\theta - \theta_w}{\theta_{fc} - \theta_w};\ \beta[0,1] \quad (3)$$

where θ is the mean volumetric soil moisture content (m^3 m^{-3}) in the root zone, θ_w is the wilting point (m^3 m^{-3}) and θ_{fc} is the field capacity (m^3 m^{-3}).

In this study we replaced Eq. (2) with the g_s model of Medlyn et al. (2011) using the same β factor as above:

$$g_s = g_0 + 1.6\left(1 + \frac{g_1\beta}{\sqrt{D}}\right)\frac{A}{C_s} \quad (4)$$

where g_1 ($kPa^{0.5}$) is a fitted parameter representing the sensitivity of the conductance to the assimilation rate. In this formulation of the g_s model, the g_1 parameter has a theoretical meaning and is proportional to:

$$g_1 \propto \sqrt{\frac{\Gamma^*}{\lambda}} \quad (5)$$

where λ is defined by Eq. (1) and Γ^* (μmol mol^{-1}) is the CO_2 compensation point in the absence of mitochondrial respiration. As a result, g_1 is inversely related to the marginal carbon cost of water, λ (Medlyn et al. 2011).

Figure 1 shows the stomatal sensitivity to D predicted by the two models in the absence of soil water stress. In this comparison, the Medlyn model has been calibrated using least squares against g_s values predicted by the Leuning model, where D varies between 0.05 and 3 kPa. The Leuning model was parameterised in the same way as the CABLE model, for C3 species: a_1 = 9.0, D_0 = 1.5 kPa and for C4 plants: a_1 = 4.0, D_0 = 1.5 kPa. The calibrated parameters for the Medlyn model were g_1 = 3.37 $kPa^{0.5}$ and g_1 = 1.10 $kPa^{0.5}$ for C3 and C4 species, respectively. Over low to moderate D ranges (<1.5 kPa), the g_s calculated by the Medlyn model declines more steeply than the Leuning model. There is then a crossover between the two models, such that at high D the Leuning model predicts g_s to be more sensitive to increasing D than the Medlyn model. We use this calibration of the Medlyn model (MED-L) to the Leuning model (LEU) throughout this manuscript, in order to distinguish structural difference between the models from differences resulting from model parameterisation (MED-P) based on a global synthesis of stomatal behaviour (see below).

189 Lin et al. (2015) compiled a global database of stomatal conductance and photosynthesis from
190 314 species across 56 field studies, which covered a wide range of biomes including Arctic
191 tundra, boreal, temperate forests and tropical rainforest. We estimated parameter values for g_1
192 for each of the 10 PFTs in CABLE (Fig. 2) by fitting Eq. (4) to this dataset, using the non-
193 linear mixed-effects model approach presented by Lin et al. (2015). We used only data from
194 ambient field conditions, excluding elevated [CO_2], temperature, or other treatments. The
195 model was fit to data for each PFT separately, using species as a random effect on the g_1
196 parameter (to account for correlation of observations within species groups). For all mixed-
197 effects models, we used the *lme4* package in R version 3.1.0 (R Core Development Team
198 2014). For this fitting, we set the parameter g_0 equal to zero. The reasons for this choice, and
199 the consequences, are discussed in detail below.

200

201 The dataset compiled by Lin et al. (2015) did not have measurements from the deciduous
202 needleleaf PFT. As Lin et al. hypothesised that the high marginal cost of water in evergreen
203 conifers is a consequence of the lack of vessels for water transport in conifer xylem, we
204 assumed that the marginal cost of water for deciduous needleleaf trees would be similar to
205 that of evergreen needleleaf.

206

207 Lin et al. (2015) also demonstrated a significant relationship ($r^2 = 0.43$) between g_1 and two
208 long-term average (1960-1990) bioclimatic variables: temperature and a moisture index
209 representing an indirect estimate of plant water availability. First, they estimated g_1 for each
210 species separately using non-linear regression, and then they fit the following equation to
211 these individual estimates of g_1:

$$\log(g_1) = a + b \times MI + c \times \bar{T} + d \times MI \times \bar{T} \quad (6)$$

212 where a, b, c, and d are model coefficients, $\bar{T}$ is the mean surface air temperature during the
213 period of the year when the surface air temperature is above 0°C, MI is a moisture index
214 calculated as the ratio of mean precipitation to the equilibrium evapotranspiration (as
215 described in Gallego-Sala et al. 2010). Equation 6 was fit using a linear mixed-effects model,
216 where PFT was used as random intercept, because we assume g_1 observations were
217 independent observations for a given PFT.

218

We derived global *MI* and $\bar{T}$ values from Climate Research Unit (CRU) CL1.0 climatology data set (1961-1990), interpolating the 0.5 degree data to 1.0 degree to match the resolution of the global offline forcing used, using a nearest neighbour approach. We masked land surface areas in the CRU data which did not correspond to one of CABLE 10 PFTs. In addition, we also masked pixels where *MI* and $\bar{T}$ estimates were not available (40 out of a possible 54,000 pixels). To directly evaluate the differences in g_1 responses to the two climatic variables amongst PFTs, we modified Eq. (6):

$$\log(g_1) = a + b\times MI + c\times\bar{T} + d\times MI\times\bar{T} + e\times\mathrm{PFT} \quad (7)$$

where *a*, *b*, *c*, *d* and *e* are model coefficients (Table, 2). We fitted Eq. (7) to the individual estimates of g_1 by species (see above), but this time with a linear regression model (because PFT here is assumed to be a fixed effect). We then used the model coefficients to predict g_1 values (MED-C) based on the PFT, *MI* and $\bar{T}$ values for each pixel. In the MED-C simulations therefore the predicted g_1 values vary within a PFT as a function of the bioclimatic indices. Standard errors of the prediction were calculated with standard methods for linear regression. Finally, we masked pixels where *MI* or $\bar{T}$ values are outside the range (*MI* > 3.26; $\bar{T}$ > 29.7°C) covered by the g_s synthesis database (126 out of a possible 54,000 pixels) to avoid extrapolation of the model.

2.3 Model simulations

In addition to the control simulation using the Leuning model (LEU), we carried out three model simulations using the Medlyn model, testing the impact of model structure (MED-L), parameterisation synthesised from experimental data (MED-P) and parameterisation based on a set of climatic indices (temperature and aridity) (MED-C) (Table 3). Simulations were first carried out at 6 flux sites selected from the FLUXNET network (http://www.fluxdata.org/) to cover a range of PFTs included in CABLE: (i) deciduous broadleaf forest; (ii) evergreen broadleaf forest; (iii) evergreen needleaf forest; (iv) C3 grassland; (v) C4 grassland; and (vi) cropland (Table 4). In both site and global simulations, each site/pixel contained only a single PFT type. Site data were obtained through the Protocol for the Analysis of Land Surface models (PALS; pals.unsw.edu.au; Abramowitz, 2012) which has previously been pre-processed and quality controlled for use within the LSM community. This process ensured

248 that all site-years had near complete observations of key meteorological drivers (as opposed
249 to significant gap-filled periods). CABLE simulations at the 6 flux sites were not calibrated to
250 match site characteristics; instead default PFT parameters were used for the appropriate PFT
251 for each site.

252

253 Next, we performed global offline simulations using the second Global Soil Wetness Project
254 (GSWP-2; Dirmeyer et al. 2006a) multi-model, 3-hourly, offline, meteorological forcing
255 (precipitation (rain and snowfall), downward shortwave and longwave radiation, surface air
256 temperature, surface specific humidity, surface wind speed and surface air pressure) over the
257 period 1986-1995 at a resolution of 1^o by 1^o with a 30-year spin-up. Although CABLE has the
258 ability to simulate carbon pool dynamics, this feature was not activated for this study, given
259 the relatively short simulation periods. For both the site-scale and global simulations, LAI
260 was prescribed using CABLE's gridded monthly LAI climatology derived from Moderate-
261 resolution Imaging Spectroradiometer (MODIS) LAI data. In all simulations, we used the
262 standard soil moisture stress function, β, defined in Eq. (3).

263

264 The GSWP-2 driven simulation used the soil and vegetation parameters similar to those
265 employed when CABLE is coupled to the ACCESS coupled model, rather than those
266 provided by the GSWP-2 experimental protocol. This was to ensure that any discrepancies
267 between different CABLE simulations could be attributed to the differences in the stomatal
268 model only. When CABLE is coupled to ACCESS model, differences in surface fluxes and
269 temperature as simulated by CABLE with different stomatal models can also influence the
270 surface forcing fields provided by the atmospheric model, which further modify the
271 simulation results by CABLE. Therefore, to ensure that the results here are comparable to
272 future ACCESS coupled simulations, we use the same soil and vegetation parameters using
273 by CABLE within ACCESS, rather than those specified by the GSWP-2 protocol.

274

275

276

2.4 Data sets for global evaluation

2.4.1 LandFlux-EVAL ET

The LandFlux-EVAL dataset (Mueller et al. 2013) provides a comprehensive ensemble of global ET estimates at a 1^{o} by 1^{o} resolution over the periods 1989-1995 and 1989-2005, derived from various satellites, LSMs driven with observationally based forcing, and atmospheric re-analysis. We used the ensemble combined product (i.e. all sources of ET and associated standard deviations) over the period 1989-1995 (that overlaps with the GSWP-2 forcing period). The rationale for comparing the simulated ET against the LandFlux-EVAL ET was to test that the uncertainties propagated to the ET estimates based on the parameterisation of g_1, were within the uncertainty range of the ensemble of existing models and observational estimates.

2.4.2 GLEAM ET

While zonal mean comparisons provide a useful measure of uncertainty, it is also useful to identify regions where the model deviates more strongly from more observational ET estimates. We therefore compared the gridded simulated seasonal ET against the latest version of the GLEAM ET product (Miralles et al. 2014). This product is an updated version of the original GLEAM ET (Miralles et al. 2011), that is part of the LandFlux-EVAL ensemble (Mueller et al. 2013). The GLEAM product assimilates multiple satellite observations (temperature, net radiation, precipitation, soil moisture, vegetation water content) into a simple land model to provide estimates of vegetation, soil and total evapotranspiration. Although estimates of vegetation transpiration are available, we only use the total ET product, as the latter has been vigorously evaluated against flux-tower measurements (Miralles et al. 2011, 2014).

2.4.3 Upscaled FLUXNET data

To estimate the influence of the new g_s parameterization on gross primary productivity (GPP), we compared our simulations against the up-scaled FLUXNET model tree ensemble (FLUXNET-MTE) dataset of Jung et al. (2009). This dataset is generated by using outputs from a dynamic global vegetation model (DGVM) forced with gridded observations as the

surrogate truth to upscale site-scale quality controlled observations. The product is more reliable where there is a high density of high quality observations, mostly restricted to North America. Nonetheless, the DGVM used to generate this product is one of the most extensively evaluated biosphere models (Jung et al. 2009). The FLUXNET dataset provides two versions of up-scaled GPP, which differ slightly in the way they are derived. We use the mean of the two products.

330 **3 Results**

331 3.1 Flux-site results

332 Figure 3 shows a site-scale comparison during daylight hours (8 am – 7 pm) between
333 observed and predicted GPP, LE and transpiration (E) at 6 FLUXNET sites. Table 5 shows a
334 series of summary statistics (RMSE, bias and index of agreement) between modelled and
335 observed LE.

336 *Impact of model structure*

337 Figure 3 shows that the differences in simulated fluxes due to model structure, shown by
338 comparing LEU with MED-L, are small across the 6 flux tower sites. Differences due to the
339 structure of the model, shown by comparing LEU with MED-L in Fig. 3, are small across
340 sites. These small differences indicate that the replacement of the Leuning model with the
341 Medlyn model (calibrated to the Leuning model, MED-L) does not significantly alter CABLE
342 simulations.

343 *Impact of new g_1 parameterisation*

344 Differences introduced by the PFT parameterisation, shown by comparing MED-P with LEU,
345 are also typically small across sites (Fig. 3), with the exception of Howard Springs (discussed
346 below) and the LE and E fluxes at Hyytiälä. At Hyytiälä, the parameterisation of a
347 conservative water use strategy for needleleaf trees leads to a reduction in both E and LE
348 fluxes (see Table 1); the change in LE is consistent with measured FLUXNET data. At
349 Bondville and Cabauw, MED-P predicts marginally higher peak fluxes as a result of a less
350 conservative water use strategy parameterisation of C3 grasses and crops, respectively.
351 Finally, for the two other sites represented by tree PFTs, Harvard and Tumbarumba, the
352 differences between modelled fluxes are negligible. The impact of g_s on LE fluxes is
353 noticeably smaller than the impact on E because modelled (and observed) LE also includes a
354 flux component from the soil.

355

356 The PFT parameterisation (MED-P) does not have a noticeable impact on predicted fluxes of
357 GPP, with the exception of Howard Springs. GPP is insensitive to the stomatal
358 parameterisation because of the non-linear relationship between g_s and A. When stomata are

fully open, A is limited by the rate of ribulose-1,5-bisphosphate (RuBP) regeneration, and is relatively insensitive to the changes in C_i caused by small reductions in stomatal conductance.

The differences between models at Howard Springs do not stem from the new g_1 parameterisation (MED-P), but instead result from the large positive g_0 parameter assumed for C4 grassland in CABLE. The assumed g_0 of 0.04 mol m^{-2} leaf s^{-1} is multiplied by LAI meaning that the minimum canopy stomatal conductance at this site can be as high as 0.1 mol m^{-2} ground s^{-1}. By contrast, in the MED-P model we assumed $g_0 = 0$, meaning that g_s goes to zero under low light and, importantly, high VPD conditions.

Figure 4 shows that at Howard Springs, high afternoon VPD caused stomatal closure, represented by reduced E, in the MED-P model but not the MED-L or LEU models (Fig. 4), due to the assumption of a high g_0 as A tends towards zero. Consequently, daily fluxes are significantly lower in the MED-P when compared to the LEU and MED-L models.

Decoupling factor

The relative insensitivity of modelled fluxes to the new g_s parameterisation (MED-P) results from CABLE's assumptions about the coupling of the vegetation to the surrounding atmosphere boundary layer. In CABLE, transpiration from the vegetation to the atmosphere is controlled by several resistances operating in series, both above (aerodynamic) and within the canopy (stomatal and leaf boundary layer), and a longwave radiative balance through radiative conductance on net available energy (Leuning et al. 1995; Kowakczyk et al. 2006). These resistances in serial, result in a relatively weak coupling between the canopy surface and the atmosphere.

Figure 5 shows the average seasonal cycle of g_s and the decoupling coefficient (Jarvis and McNaughton, 1985; McNaughton and Jarvis, 1991) simulated by CABLE at the 6 flux tower sites. The decoupling coefficient (Ω) represents how well coupled the vegetation is to the surrounding atmosphere, with a value of 0 representing fully coupled behaviour, where transpiration is controlled by g_s, and a value of 1 representing completely decoupled behaviour, where transpiration is controlled by the available energy. The moderate to high Ω

389 at all sites, with the exception of Hyytiälä, explains the lack of sensitivity in the E, LE and
390 GPP fluxes to changes in g_s. At Hyytiälä, Ω is low, and becomes lower when g_1 is reduced in
391 the MED-P model, resulting in an effect on E is more apparent than at the other sites (see Fig.
392 3).

393

394 3.2 Global results

395 *Global maps of g_1*

396 To facilitate global comparisons, we have derived global maps of the g_1 parameter. Figure 6a
397 shows a clear latitudinal gradient, with lower values of g_1, which represent a more
398 conservative water use strategy, found in mid-latitudes (20-60°N), whilst higher values of g_1
399 are located towards more tropical regions. When within-PFT variation with bioclimatic
400 indices is included (Fig. 6b) there is more variability in g_1, particularly across the tropics, due
401 to spatial variability in temperature. Parameter uncertainty maps (± 2 standard errors) of the g_1
402 parameter are shown in Fig. S1. These maps indicate considerable uncertainty in deriving the
403 g_1 parameter as a function of these climate relationships (Fig. S1c,d), particularly for C3
404 grasses (mean (μ) range = 1.42−8.80) and C3 crops (μ range = 3.99−8.89) PFTs.

405

406 *Impact of model structure on simulated GPP and E*

407 We next extend our comparison by examining the impact of different stomatal conductance
408 models on the simulated seasonal and annual GPP and E, the fluxes most directly impacted by
409 g_s in the model. Figures 7 and 8 show mean seasonal (December–January–February: DJF, and
410 June–July–August: JJA) difference maps of predicted GPP and E, respectively. Tables 6 and
411 7 summarise changes in GPP and E in terms of mean annual totals across all the GSWP-2
412 years. Similar to Fig. 3, changes in simulated fluxes due to the different model structure
413 (shown by LEU−MED-L, Figs. 7a, b and 8a, b), are typically small (μ change in GPP and E
414 relative to the control (LEU) < 7 %, with the exception of the shrub PFT, which has μ ~12 %).
415 The largest differences (relative to the LEU) in GPP occur over grass (C3 GPP μ = 47.7 gC m^{-2} y^{-1}, μ change = 4.6 %; C4 GPP μ = 93.0 gC m^{-2} y^{-1}, μ change = 5.6%) and shrub PFTs (GPP
417 μ = 69.3 gC m^{-2} y^{-1}, μ change = 12 %), where the LEU model predicts higher fluxes (Figs.

418 7a,b). Figures 8a and b shows that the largest differences (relative to the LEU) in E occur
419 across the tropics, where fluxes in broadleaf forest PFTs are higher (E μ = 34.3 mm y^{-1}, μ
420 change = 5.5 %) in the MED-L model. These differences are consistent with the different
421 sensitivities of the modelled stomatal conductance to *D*, as show in Fig. 1. The LEU model
422 would tend to predict higher g_s fluxes at low to moderate *D* (<2 kPa), whereas the calibrated
423 MED-L model would predict higher g_s fluxes at moderate to high *D* (>2kPa).

424

425 *Impact of empirically fitted g_1 parameterisation on the simulated GPP and E*

426 The key differences introduced by the MED-P model (Figs. 7c, d and 8c, d) are 29 %
427 reduction in E relative to the control (MED-C) simulation for evergreen needleleaf, C4 grass
428 and Tundra PFTs. Fluxes were reduced across the boreal zone (E μ = 76.1 mm y^{-1}), over C4
429 grass areas (GPP μ = 302.9 gC m^{-2} y^{-1}, μ change = 16.5 %; E μ = 107.7 mm y^{-1}, μ change =
430 27.1 %) and the tundra PFT (E μ = 24.1 mm y^{-1}, μ change = 28.5 %). Fluxes are also
431 predicted to decrease over deciduous needleleaf PFTs, but this result should be viewed with
432 caution, as this was the PFT for which there were no synthesis data available. As such, this
433 result just reflects the assumption that these PFTs behave in the same way as evergreen
434 needleleaf PFTs. The MED-P model also predicts increases over regions of C3 crop (GPP μ =
435 64.9 gC m^{-2} y^{-1}, μ change = 5.5 %; E μ = 30 mm y^{-1}, μ change = 10.9 %) and C3 grasses (GPP
436 μ = 66.8 gC m^{-2} y^{-1}, μ change = 5.9 %; E μ = 17.4 mm y^{-1}, μ change = 7.6 %).

437

438 *Impact of predicted g_1 parameterisation on the simulated GPP and E*

439 Figures 7e,f and 8e,f show the predicted fluxes when g_1 is allowed to vary within a PFT
440 according to climate indices. Generally, the changes are in line with the changes introduced
441 by the MED-P parameterisation. The largest change is a 32 % reduction in E relative to the
442 control simulation for evergreen needleleaf pixels. The notable difference compared to the
443 MED-P simulation occurs over C4 grass pixels. The MED-C model predicts fluxes that are
444 approximately half those predicted by the MED-P model for both GPP and E. This suggests a
445 less conservative water use strategy than is obtained through the PFT-specific
446 parameterisation alone, i.e. MED-P.

3.3 Comparison with benchmarking products

Global simulations by the CABLE model using different models of stomatal conductance were compared to the FLUXNET-MTE GPP and GLEAM ET data products (not shown). Differences between these data products and CABLE simulations generally are much larger than the differences among different CABLE simulations with different stomatal conductance model (MED-P/C). Both products suggest that CABLE over-predicts GPP across the globe and ET across mid-latitudes (20-60°N). The MED-P/C models slightly improve agreement with the FLUXNET-MTE GPP (Table 8) and GLEAM ET for the evergreen needleleaf PFT (Table 9). Agreement is also improved for C4 grasses and Tundra PFTs. However, when considering all PFTs, the MED-P/C models do not noticeably improve agreement with the GLEAM or FLUXNET-MTE products.

Figure 9 shows zonal means by latitude for DJF and JJA compared to the upscaled FLUXNET-MTE GPP and LandFlux-EVAL ET products. As described above, across all latitudes, the differences between the GPP from the data products and those fluxes predicted by the models (LEU, MED-P and MED-C) are generally large and the impact of the new stomatal scheme is typically negligible (Figs. 8a,b). By contrast, the comparison with ET from the observational data product (Figs. 8c,d) is broadly consistent across all latitudes. Notably, in JJA, the lower ET fluxes predicted by the MED-P/C models across mid (20-60°N) to high latitudes (> 60°N) are in agreement with the LandFlux-EVAL product, though the modelled ET from the MED-L model is not outside the uncertainty envelope of the product. In DJF, the MED-P model also predicts lower GPP and ET fluxes across the tropics (20°S-20°N) which would be towards the low end of the uncertainty envelope from the LandFlux-Eval product, but still falls outside the uncertainty range of FLUXNET-MTE.

4 Discussion

4.1 Optimisation theory in LSMs

In this study we have implemented a simple stomatal conductance model, which was derived using optimisation theory, into a LSM. By calibrating parameters to match the existing parameterisation of the original empirical stomatal model (MED-L), we were able to show that the new model structure for stomatal conductance does not degrade overall model performance. This result is similar to that of Bonan et al. (2014), who implemented the optimal stomatal conductance scheme into the CLM LSM, following Williams et al. (1996). In their implementation they solve the optimisation problem numerically (Eq. 1), with the additional assumption that leaf water potential cannot fall below a minimum value, effectively replacing the empirical soil water scalar used here (Eq. 3). Our results and those of Bonan et al. (2014) demonstrate that model performance using the optimisation scheme was comparable to the original empirical stomatal conductance (Ball et al. 1987) scheme.

Optimisation of key plant attributes is a viable alternative to empirical or overly complex mechanistic model algorithms (Dewar et al. 2009). Optimisation is readily achieved via numerical methods, but these are typically computationally intensive, which is a concern for models used in long-term climate projections. Analytical approximations to optimisation such as the stomatal conductance model used here (Medlyn et al. 2011) provide an operational alternative. In this instance, the analytical solution is preferable to the numerical optimisation because it correctly captures stomatal responses to rising atmospheric CO_2 concentration, whereas the full numerical solution does not. In the full numerical solution, optimal stomatal behaviour differs depending on whether RuBP regeneration or Rubisco activity is limiting photosynthesis, and the predicted CO_2 response is incorrect when Rubisco activity is limiting, unless the stomatal slope g_1 is assumed to vary with atmospheric CO_2 (Katul et al. 2010; Medlyn et al. 2013). The analytical solution, in contrast, assumes that stomatal behaviour is regulated as if photosynthesis were always RuBP-regeneration-limited, which yields the correct CO_2 response.

506 The advantage of using an analytical model based on optimisation theory rather than an
507 empirical model is that it provides a basis for model parameterisation. Our implementation of
508 the optimal model has one key parameter, g_1, which is related to the marginal carbon cost of
509 water. It is possible to use theoretical considerations to predict how this parameter should
510 vary among PFTs and with mean annual climate (e.g. Prentice et al. 2014; Lin et al. 2015).
511 The parameter can also be readily and accurately estimated from data, meaning that the
512 predicted parameter values can be tested. For example, Héroult et al. (2013) predicted and
513 demonstrated a negative correlation between the g_1 parameter and wood density, and a
514 positive correlation with the root-to-leaf hydraulic conductance. Lin et al. (2015) examined
515 these relationships with their global stomatal dataset and concluded that such a relationship is
516 consistent across angiosperm tree species but not gymnosperm species.

517

518 In this study we extended the work of Lin et al. (2015) by predicting g_1 values as a function of
519 bioclimatic variables (temperature and aridity) (MED-C). The estimated parameter values
520 were employed in the LSM and resulted in large changes to predicted fluxes in evergreen
521 needleleaf and C4 vegetation. We have highlighted how the key stomatal conductance
522 parameter could in theory be predicted, rather than calibrated, or, alternatively, linked to other
523 traits (wood density) in the model. This work paves the way for broader implementations of
524 optimisation theory in LSMs and other large-scale vegetation models.

525

526 As g_1 represents plant water use strategy, there is also potential to hypothesise how it may
527 vary during drought. Inadequate simulation of soil moisture availability by LSMs is often
528 identified as a key weakness in surface flux prediction (Gedney et al. 2000; Dirmeyer et al.
529 2006b; Lorenz et al. 2012; De Kauwe et al. 2013b). In LSMs, as soil moisture declines, gas
530 exchange is typically reduced through an empirical scalar (Wang et al. 2011) accounting for
531 change in soil water content, but not plant behaviour (isohydric vs. anisohydric) (Egea et al.
532 2011). Bonan et al. (2014) showed that during drought periods, the formulation of the soil
533 moisture stress scalar was likely to be the cause of error in g_s calculations, rather than the g_s
534 scheme itself. Zhou et al. (2013, 2014) demonstrated that the g_1 parameter could be linked to
535 a more theoretical approach to limit gas exchange during water-limited periods, by
536 considering differences in species water use strategies.

4.2 Performance of the new model and parameterisation

We tested an implementation of a new stomatal conductance model within the CABLE LSM, at site and global scales to assess the impact on the simulated carbon, water and energy fluxes. We utilised a dataset that synthesised stomatal behaviour across the globe in order to constrain g_1 for each PFT (MED-P). In addition, we demonstrated that g_1 can be predicted from bioclimatic temperature and aridity datasets and tested the impact of model simulations using this parameterisation (MED-C).

Introducing the Medlyn g_s model with g_1 parameterisations (MED-P/C) to the CABLE LSM resulted in reductions in E of ~30 % compared to the standard CABLE simulations across evergreen needleleaf, tundra and C4 grass regions (Figs. 7c-f and 8c-f). This large difference represents the conservative behaviour of these PFTs as reported by Lin et al. (2015), currently not captured by the standard CABLE parameters. In other regions of the globe, the differences between fluxes predicted by the models was typically small (Figs. 7, 8 and Tables 6 and 7). Changes of ~30% in E across evergreen needleleaf, tundra and C4 grass PFTs has the potential to affect regional and conceivably global scale climate.

In comparison to the LandFlux-EVAL ET product, across mid to high latitudes, the ET predicted by the MED-P/C models is closer to the mean of the LandFlux-EVAL products, though the LEU simulations were still within the uncertainty range of the ensemble (Fig. 9). Across the tropics, the MED-P model predicted a reduction in ET fluxes when compared with LandFlux-EVAL estimate and the LEU model, however simulations were still within the uncertainty envelope. Interestingly, over this region the MED-C scheme predicted fluxes closer to the LEU model than the MED-P. Lorenz et al. (2014) showed that CABLE, when coupled to ACCESS, predicted excessive ET across much of the northern hemisphere, leading to unrealistically small diurnal temperature ranges. The new stomatal parameterisation predicts reduced transpiration across northern latitudes (Figs. 8d and 9d). We note that this only results in a small improvement in the spatial agreement when compared with the GLEAM ET product (Table 9), suggesting that there are other causes not related to g_s for the model-data bias.

Across all latitudes, the changes introduced by the new stomatal scheme did not degrade the agreement with the FLUXNET-MTE GPP data product (Table, 8), although it was notable that CABLE over-predicted (outside the uncertainty range) GPP across the tropics. The MED-P model did predict lower GPP fluxes for this region and the direction of the change was supported by the data product, but the change in fluxes was small and still outside the uncertainty range of the FLUXNET-MTE product. Data from Lin et al. (2015) for 3 species in the Amazon suggests that a g_1 value of 4.23 $kPa^{0.5}$ would be appropriate, which is close to the PFT derived evergreen broadleaf value used in MED-P simulations (4.12 $kPa^{0.5}$). This line of evidence, in combination with the GPP over-prediction, would tend to suggest that the mismatch between model and data stems from other biases (in model and/or forcing) unrelated to g_s. Zhang et al. (2013) previously identified a bias in predicted ET and runoff fluxes from CABLE over the Amazon region, but argued that this bias was unlikely to result from the meteorological forcing data.

Another avenue of potential bias may relate to the use of a prescribed (as is typical in LSMs) MODIS LAI climatology, which has been reported to be inaccurate over forested regions (Shabanov et al. 2005; De Kauwe et al. 2011; Sea et al. 2011; Serbin et al. 2013). The sensitivity to stomatal parameterisation may be larger when using prognostic LAI. In prognostic LAI simulations there may be feedbacks from changes in g_s to LAI that could cause larger differences between the Medlyn and the standard Leuning model, both in terms of the different timings of predicted flux maximums and associated feedbacks on carbon and water fluxes. We cannot resolve these wider issues of model bias here, but these issues warrant further investigation.

4.3 Implications for other models

We anticipate that the new stomatal model could also be readily incorporated into other LSMs. However, other LSMs may show more or less sensitivity to the introduction of a new stomatal model and parameters, depending on how they represent boundary layer conductance. Models with low boundary layer conductance will have low stomatal control of fluxes, and highly decoupled canopies, whereas models with relatively high boundary layer conductance will have strong stomatal control and highly coupled canopies.

De Kauwe et al. (2013) previously showed decoupling to be a key area of disagreement between 11 ecosystem models. In this comparison, CABLE appeared as a relatively decoupled model because it considers multiple conductances in series, including aerodynamic (above the canopy), boundary layer (within the canopy), and a radiative conductance, accounting for differences in longwave radiation balance between isothermal and non-isothermal conditions (Wang and Leuning, 1998). In comparison, some other LSMs, for example the Joint UK Land Environment Simulator (JULES; Best et al. 2011; Cox et al. 1999) and O-CN (Zaehle and Friend, 2010), only consider a bulk aerodynamic conductance term, and thus would typically predict considerably more coupling. Therefore, such LSMs would predict a larger influence of changes in stomatal conductance than CABLE. This sensitivity was demonstrated by Booth et al. (2012), who used the Met Office Surface Exchange System (MOSES; from which JULES was developed) to highlight that the stomatal conductance parameter was a key driver of uncertainty in future estimates of the atmospheric concentration of CO_2 from a coupled carbon cycle model (HadCM3C). They showed that by perturbing the stomatal slope parameter (i.e. g_1 in our notation), their model predicted a large uncertainty in the 1900 to 2100 atmospheric CO_2 change of between 380 to 850 ppm. The Ecosystem Demography model v2 (ED2; Medvigy et al. 1999) is another relatively coupled model, with high sensitivity to g_s. Dietze et al. (2014) estimated that that ~10 % of the uncertainty in net primary productivity (NPP) predicted by the ED2 model across North America Biomes was directly due to the stomatal slope parameter (i.e. g_1). This uncertainty was found to be largest in the evergreen PFTs (~21 %), whereas estimates of NPP from grassland PFTs were largely insensitive. It is clear that levels of coupling between the canopy and the atmosphere vary between LSMs and this presents a key area of model uncertainty.

Determining the appropriate level of decoupling is not a trivial task. Previous estimates of the decoupling coefficient (Ω) based on flux data have either estimated the aerodynamic resistance from the wind speed and the friction velocity u^* (e.g. Lee and Black 1993; Hasler and Avissar, 2006), or from wind speed, stand height and roughness length (e.g. Stoy et al. 2006); both approaches ignore within-canopy turbulence. Launiainen et al. 2010 reported an average (1997-2008) July-August $\Omega = 0.32$ (standard deviation = 0.07) for the Hyytiälä site. By comparison, CABLE predicted a more coupled canopy, July-August (1996-2006) Ω =

0.21 (standard deviation = 0.11) from the standard Leuning model. Other literature studies for coniferous forests suggest a lower $\Omega \sim 0.1$-0.2 (Jarvis 1985; Jarvis and McNaughton 1986; Lee and Black, 1993; Meinzer 1993). Ranges suggested for other PFTs are typically broad; between 0.5-0.9 for broadleaf tropical forest species (Meinzer 1993; Meinzer et al., 1997; Wullschleger et al. 1998; Cienciala et al. 2000) and 0.4-0.9 for crops (Meinzer 1993). This broad range in Ω makes it difficult to conclude which LSM most correctly simulates coupling. However, as a major source of disagreement among models, we emphasise that coupling strength is an important issue to address.

4.4 Minimum stomatal conductance, g_0

The empirical Leuning g_s model includes a minimum stomatal conductance term, g_0. This term can also be added to the optimal Medlyn model. The value of this parameter can have a significant impact on predicted ecosystem fluxes, as we found at the Howard Springs site (Figs. 3 and 4). The values used in the standard CABLE model ($g_0 = 0.01$ and 0.04 mol m^{-2} s^{-1} for C3 and C4 species respectively) were taken from the Simple Biosphere Model version 2 (SiB2) (Sellers et al. 1996), but the original source of these parameter values is unclear. Replacing these values with zeroes had a large impact on predicted fluxes, particularly under high VPD conditions at the C4-dominated Howard Springs. This result agrees with a recent study by Barnard and Bauerle (2013), who concluded that g_0 was in fact the most sensitive parameter for correctly estimating transpiration fluxes. It is clear that further investigation is needed on the impact of different g_0 assumptions in land surface and ecosystem models. Here we offer some thoughts about the directions such investigations could take.

First, it will be important to query the way in which g_0 is incorporated into the stomatal model. Adding a g_0 term as a model intercept, as is currently done, is not based on theory, and has the unintended consequence that it affects predicted stomatal conductance at all times, not only when photosynthesis approaches zero, resulting in high sensitivity to this model parameter. Alternative model structures incorporating g_0 can be derived depending on what g_0 is assumed to represent. If we assume, for example, that g_0 represents a physical lower limit to stomatal conductance, below which it is not possible for g_s to fall, the optimal behaviour would be for g_0 to be a lower bound to stomatal conductance predicted by the standard model. Thus, an alternative model structure to consider would be the maximum of g_0 and the optimal

662 g_s, rather than the sum of the two.

663 It will also be important to carefully consider how to parameterise the value of g_0. Some
664 authors suggest using night-time stomatal conductance values (e.g. Zeppel et al. 2014).
665 However, minimum stomatal conductance values measured during the day are considerably
666 lower than measured night-time values (Walden-Coleman et al. 2013). We extracted the
667 minimum g_s values for each species from the dataset of Lin et al. (2015) and plotted them as a
668 function of the minimum recorded photosynthesis values (Fig. S2). It can be seen that the
669 minimum g_s values tend to zero with minimum recorded A, and are much lower than the
670 values currently assumed in CABLE and the night-time g_s values estimated from the literature
671 by Zeppel et al. (2014). Consequently, we suggest that values of g_0 used in the stomatal model
672 applied during the day should be estimated from daytime, rather than night-time
673 measurements.

674

675

676 **Acknowledgements**

677 This work was supported by the Australian Research Council Centre of Excellence for
678 Climate System Science through grant CE110001028, and by ARC Discovery Grant DP
679 DP120104055. This study uses the LandFlux-EVAL merged benchmark synthesis products of
680 ETH Zurich produced under the aegis of the GEWEX and ILEAPS
681 projects (http://www.iac.ethz.ch/url/research/LandFluxEVAL/). We thank CSIRO and the
682 Bureau of Meteorology through the Centre for Australian Weather and Climate Research for
683 their support in the use of the CABLE model. We thank the National Computational
684 Infrastructure at the Australian National University, an initiative of the Australian
685 Government, for access to supercomputer resources. The up-scaled Fluxnet dataset was
686 provided by Martin Jung from the Max Planck Institute for Biogeochemistry. This work used
687 eddy covariance data acquired by the FLUXNET community for the La Thuile FLUXNET
688 release, supported by the following networks: AmeriFlux (U.S. Department of Energy,
689 Biological and Environmental Research, Terrestrial Carbon Program (DE-FG02-04ER63917
690 and DE-FG02-04ER63911)), AfriFlux, AsiaFlux, CarboAfrica, CarboEuropeIP, CarboItaly,
691 CarboMont, ChinaFlux, Fluxnet-Canada (supported by CFCAS, NSERC, BIOCAP,
692 Environment Canada, and NRCan), GreenGrass, KoFlux, LBA, NECC, OzFlux, TCOS-

Siberia, USCCC. We acknowledge the financial support to the eddy covariance data harmonization provided by CarboEuropeIP, FAO-GTOS-TCO, iLEAPS, Max Planck Institute for Biogeochemistry, National Science Foundation, University of Tuscia, Université Laval and Environment Canada and US Department of Energy and the database development and technical support from Berkeley Water Center, Lawrence Berkeley National Laboratory, Microsoft Research eScience, Oak Ridge National Laboratory, University of California - Berkeley, University of Virginia. D.G.M. acknowledges financial support from Netherlands Organisation for Scientific Research (NWO) through grant 863.14.004. All data analysis and plots were generated using the Python language and the Matplotlib Basemap Toolkit (Hunter, 2007).

720 **References**

721 Abramowitz, G., Leuning, R., Clark, M., Pitman, A., 2008. Evaluating the Performance of
722 Land Surface Models. J. Clim. 21, 5468–5481.

723

724 Abramowitz, G. (2012) Towards a public, standardized, diagnostic benchmarking system for
725 land surface models, Geoscientific Model Development, 5, 819-827, doi:10.5194/gmd-5-819-
726 2012.

727

728 Aphalo, P., Jarvis, P., 1991. Do stomata respond to relative humidity? Plant Cell Environ. 14,
729 127–132.

730

731 Arneth, A., Lloyd, J., Šantrůčková, H., Bird, M., Grigoryev, S., Kalaschnikov, Y., Gleixner,
732 G., Schulze, E.-D., 2002. Response of central Siberian Scots pine to soil water deficit and
733 long-term trends in atmospheric CO2 concentration. Glob. Biogeochem. Cycles 16, 5–1.

734

735 Ball, M.C., Woodrow, I.E., Berry, J.A., 1987. Progress in Photosynthesis Research, in:
736 Biggins, I. (Ed.), Martinus Nijhoff Publisheres, Netherlands, pp. 221–224.

737

738 Barnard, D., Bauerle, W., 2013. The implications of minimum stomatal conductance on
739 modeling water flux in forest canopies. J. Geophys. Res. Biogeosciences., 118, 1322-1333.

740

741 Beringer, J., Hutley, L.B., Tapper, N.J., Cernusak, L.A., 2007. Savanna fires and their impact
742 on net ecosystem productivity in North Australia. Glob. Change Biol. 13, 990–1004.

743

744 Betts, R.A., Boucher, O., Collins, M., Cox, P.M., Falloon, P.D., Gedney, N., Hemming, D.L.,
745 Huntingford, C., Jones, C.D., Sexton, D.M., Webb, M.J., 2007. Projected increase in
746 continental runoff due to plant responses to increasing carbon dioxide. Nature 448, 1037–
747 1041.

748

749 Best, M.J., Pryor, M., Clark, D.B., Rooney, G.G., Essery, R.L.H., Ménard, C.B., Edwards,
750 J.M., Hendry, M.A., Porson, A., Gedney, N., Mercado, L.M., Sitch, S., Blyth, E., Boucher,
751 O., Cox, P.M., Grimmond, C.S.B., Harding, R.J., 2011. The Joint UK Land Environment
752 Simulator (JULES), model description – Part 1: Energy and water fluxes. Geosci. Model Dev.
753 Discuss. 4, 595–640.

754

755 Booth, B.B., Jones, C.D., Collins, M., Totterdell, I.J., Cox, P.M., Sitch, S., Huntingford, C.,
756 Betts, R.A., Harris, G.R., Lloyd, J., 2012. High sensitivity of future global warming to land
757 carbon cycle processes. Environ. Res. Lett. 7, 024002.

758

759 Bonan, G., Williams, M., Fisher, R., Oleson, K., 2014. Modeling stomatal conductance in the
760 Earth system: linking leaf water-use efficiency and water transport along the soil-plant-
761 atmosphere continuum. Geosci. Model Dev. Discuss. 7, 3085–3159.

762

763 Buckley, T., Mott, K., Farquhar, G., 2003. A hydromechanical and biochemical model of
764 stomatal conductance. Plant Cell Environ. 26, 1767–1785.

765

766 Cao, L., Bala, G., Caldeira, K., Nemani, R., Ban-Weiss, G., 2010. Importance of carbon
767 dioxide physiological forcing to future climate change. Proc. Natl. Acad. Sci. U. S. A. 107,
768 9513–9518.

769

770 Cox, P., Betts, R., Bunton, C., Essery, R., Rowntree, P., Smith, J., 1999. The impact of new
771 land surface physics on the GCM simulation of climate and climate sensitivity. Clim. Dyn.
772 15, 183–203.

773

774 Cienciala, E., Kučera, J., Malmer, A., 2000. Tree sap flow and stand transpiration of two
775 *Acacia mangium* plantations in Sabah, Borneo. J. Hydrol. 236, 109–120.

776

777 Cowan, I., Farquhar, G., others, 1977. Stomatal function in relation to leaf metabolism and
778 environment, in: Symposia of the Society for Experimental Biology. p. 471.

779

780 Cowan, I.R. 1982. Regulation of water use in relation to carbon gain in higher plants. In
781 Encyclopedia of Plant Physiology, New Series. Vol. 12B. Eds. O.L. Lange, P.S. Nobel and
782 C.B. Osmond. Springer-Verlag, Berlin. pp 589-613.

783

784 Cruz, F.T., Pitman, A.J., Wang, Y.-P., 2010. Can the stomatal response to higher atmospheric
785 carbon dioxide explain the unusual temperatures during the 2002 Murray-Darling Basin
786 drought? J. Geophys. Res. Atmospheres 1984–2012 115.

787

788 Damour, G., Simonneau, T., Cochard, H., Urban, L., 2010. An overview of models of
789 stomatal conductance at the leaf level. Plant Cell Environ. 33, 1419–1438.

790

791 De Kauwe, M.G., Medlyn, B.E., Zaehle, S., Walker, A.P., Dietze, M.C., Hickler, T., Jain,
792 A.K., Luo, Y., Parton, W.J., Prentice, C., others, 2013a. Forest water use and water use
793 efficiency at elevated CO2: a model-data intercomparison at two contrasting temperate forest
794 FACE sites. Glob. Change Biol. 19, 1759–1779.

795

796 De Kauwe, M.G., Taylor, C.M., Harris, P.P., Weedon, G.P., Ellis, R.J., 2013b. Quantifying
797 land surface temperature variability for two Sahelian mesoscale regions during the wet
798 season. J. Hydrometeor, 14, 1605-1619.

799

800 Dewar, R., Franklin, O., Mäkelä, A., Mcmurtrie, R., Valentine, H., 2009. Optimal Function
801 Explains Forest Responses to Global Change. Biosci., 59, 127–139.

802

803 Dickinson, R.E., Shaikh, M., Bryant, R., Graumlich, L., 1998. Interactive canopies for a
804 climate model. J. Clim. 11, 2823–2836.

805

806 Dietze, M. C., Serbin, S. P., Davidson, C., Desai, A. R., Feng, X., Kelly, R., Kooper,

807 R., LeBauer, D., Mantooth, J., McHenry, K. Wang, D. 2014, A quantitative assessment of a
808 terrestrial biosphere model's data needs across North American biomes, J. Geophys. Res.
809 Biogeosciences, 119, 286–300.

810

811 Dirmeyer, P.A., Gao, X., Zhao, M., Guo, Z.H., Oki, T., Hanasaki, N., 2006a. GSWP-2-
812 multimodel analysis and implications for our perception of the land surface. B. Am. Meteorol.
813 Soc., 87, 1381-1397.

814

815 Dirmeyer, P. A., Koster, R. D., Guo, Z. 2006b, Do global models properly represent the
816 feedback between land and atmosphere? J. Hydrometeor., 7, 1177-1198.

817

818 Duursma, R.A., Payton, P., Bange, M.P., Broughton, K.J., Smith, R.A., Medlyn, B.E., Tissue,
819 D.T., 2013. Near-optimal response of instantaneous transpiration efficiency to vapour
820 pressure deficit, temperature and [CO2] in cotton (Gossypium hirsutum L.). Agricultural and
821 Forest Meteorology 168, 168–176

822

823

824 Egea, G., Verhoef, A., Vidale, P.L., 2011. Towards an improved and more flexible
825 representation of water stress in coupled photosynthesis–stomatal conductance models. Agric.
826 For. Meteorol. 151, 1370–1384.

827

828 Farquhar, G.D., Sharkey, T.D., 1982. Stomatal conductance and photosynthesis. Annu. Rev.
829 Plant Physiol. 33, 317–345.

830

831 Gallego-Sala, A., Clark, J., House, J., Orr, H., Prentice, I.C., Smith, P., Farewell, T.,
832 Chapman, S., 2010. Bioclimatic envelope model of climate change impacts on blanket
833 peatland distribution in Great Britain. Clim. Res. 45, 151–162.

834

Gedney, N., Cox, P., Douville, H., Polcher, J., Valdes, P., 2000. Characterizing GCM land surface schemes to understand their responses to climate change. J. Clim. 13, 3066–3079.

Gedney, N., Cox, P., Betts, R., Boucher, O., Huntingford, C., Stott, P., 2006. Detection of a direct carbon dioxide effect in continental river runoff records. Nature 439, 835–838.

Hari, P., Mäkelä, A., Korpilahti, E., Holmberg, M., 1986. Optimal control of gas exchange. Tree Physiol. 2, 169–175.

Hasler, N., Avissar, R. 2006. What controls evapotranspiration in the Amazon Basin? J. Hydrometeor, 8, 380–395.

Henderson-Sellers, A., McGuffie, K., Gross, C., 1995. Sensitivity of global climate model simulations to increased stomatal resistance and CO_2 increases. J. Clim. 8, 1738-1756.

Héroult, A., LIN, Y.-S., Bourne, A., Medlyn, B.E., Ellsworth, D.S., 2013. Optimal stomatal conductance in relation to photosynthesis in climatically contrasting Eucalyptus species under drought. Plant Cell Amp Environ. 36, 262–274.

Hunter, J.D., 2007. Matplotlib: A 2D graphics environment. Comput. Sci. Amp Eng. 9, 90–95.

Jarvis, P., 1976. The interpretation of the variations in leaf water potential and stomatal conductance found in canopies in the field. Philos. Trans. R. Soc. Lond. B. Biol. Sci. 273, 593–610.

Jarvis, P.G., 1985. Attributes of Trees as Crop Plants, in: Cannell, M.G.R., Jackson, J.E. (Eds.), Attributes of Trees as Crop Plants. Institute of Terrestrial Ecology, pp. 460–480.

Jarvis, P., McNaughton, K., 1986. Stomatal control of transpiration: Scaling up from leaf to region. Adv. Ecol. Res. 15, 1–49.

Jasechko, S., Sharp, Z.D., Gibson, J.J., Birks, S.J., Yi, Y., Fawcett, P.J., 2013. Terrestrial water fluxes dominated by transpiration. Nature 496, 347–350.

Jung, M., Reichstein, M., Bondeau, A., 2009. Towards global empirical upscaling of FLUXNET eddy covariance observations: validation of a model tree ensemble approach using a biosphere model. Biogeosciences 6, 2001–2013.

Kala, J., Decker, M., Exbrayat, J.-F., Pitman, A.J., Carouge, C., Evans, J.P., Abramowitz, G., Mocko, D., 2014. Influence of Leaf Area Index Prescriptions on Simulations of Heat, Moisture, and Carbon Fluxes. J. Hydrometeorol. 15, 489–503.

Katul, G.G., Palmroth, S., Oren, R., 2009. Leaf stomatal responses to vapour pressure deficit under current and CO_2-enriched atmosphere explained by the economics of gas exchange. Plant Cell Environ. 32, 968–979

Kerstiens, G., 1996. Cuticular water permeability and its physiological significance. J. Exp. Bot. 47, 1813–1832.

Kowalczyk, E.A., Wang, Y.P., Wang, P., Law, R.H., Davies, H.L., 2006. The CSIRO Atmosphere Biosphere Land Exchange (CABLE) model for use in climate models and as an offline model (No. CSIRO Marine and Atmospheric Research paper 013). CSIRO.

Kowalczyk, E. A., Stevens, L., Law, R. M., Dix, M. D., Wang, Y-P., Harman, I. N., Haynes, K., Srbinovsky, J., Pak, B. and Ziehn, T. (2013) The land surface model component of ACCESS: description and impact on the simulated surface climatology. Australian Meteorological and Oceanographic Journal, 63, 65-82.

894 Krinner, G., Viovy, N., de Noblet-Ducoudré, N., Ogée, J., Polcher, J., Friedlingstein, P.,
895 Ciais, P., Sitch, S., Prentice, I.C., 2005. A dynamic global vegetation model for studies of the
896 coupled atmosphere-biosphere system. Glob. Biogeochem. Cycles 19, GB1015.

897

898 Launiainen, S.2010. Seasonal and interannual variability of energy exchange above a boreal
899 Scots pine foest. Biogeosci. 7, 3921–3940.

900

901 Lee, X. and Black, T.A. 1993. Atmospheric turbulence within and above a Douglas fir stand.
902 Part II: eddy fluxes of sensible heat and water vapour. Boundary Layer Meteorol, 64, 369–
903 389.

904

905 Leuning, R., 1995. A critical appraisal of a combined stomatal-photosynthesis model for C_3
906 plants. Plant Cell Environ. 18, 339–355.

907

908 Lin, Y.-S., Medlyn, B. E., Duursma, R. A., Prentice, I. C., Wang, H., Baig, S., Eamus, D.,
909 Resco de Dios, V. Mitchell, P., Ellsworth, D. S., Op de Beeck, M., Wallin, G., Uddling, J.,
910 Tarvainen, L., Linderson, M-J., Cernusak, L. A., Nippert, J. B., Ocheltree, T. W., Tissue. D.
911 T., Martin-StPaul, N. K., Rogers, A., Warren, J. M., De Angelis, P, Hikosaka, K., Han, Q.,
912 Onoda, Y., Gimeno, T. E., Barton, C. V. M., Bennie, J., Bonal, D., Bosc, A., Löw, M.,
913 Macinins-Ng, C., Rey, A., Rowland, L., Setterfield, S. A., Tausz-Posch, S., Zaragoza-
914 Castells, J., Broadmeadow, M. S. J., Drake, J. E., Freeman, M., Ghannoum, O., Hutley, L. B.,
915 Kelly, J. W., Kikuzawa, K., Kolari, P., Koyama, K., Limousin, J-M., Meir, P., Lola da Costa,
916 A. C., Mikkelsen, T. N., Norma Salinas, Sun, W., 2015. Optimal stomatal behaviour around
917 the world: synthesis of a global stomatal conductance database. Nature Clim. Change, in
918 press.

919

920 Lloyd J. 1991. Modeling stomatal responses to environment in Macadamia integrifolia. Aust.
921 J. Plant Physiol., 18, 649-660.

922

923 Lorenz, R., Pitman, A., Donat, M., Hirsch, A., Kala, J., Kowalczyk, E., Law, R., Srbinovsky,
924 J., 2014. Representation of climate extreme indices in the ACCESS1. 3b coupled atmosphere-
925 land surface model. Geosci. Model Dev. 7, 545–567.
926
927 Lu, X.J., Wang, Y.P., Ziehn, T. and Dai, Y.J. (2013). An efficient method for global
928 parameter sensitivity analysis and its applications to the Australian community land surface
929 models (CABLE). Agric. For. Meteorol, 182-183:292-303.
930
931 McNaughton, K., Jarvis, P., 1991. Effects of spatial scale on stomatal control of transpiration.
932 Agric. For. Meteorol. 54, 279–302.
933
934 Medlyn, B.E., Duursma, R.A., De Kauwe, M.G., Prentice, I.C., 2013. The optimal stomatal
935 response to atmospheric CO2 concentration: Alternative solutions, alternative interpretations.
936 Agric. For. Meteorol., 182-183, 200-203.
937
938 Medlyn, B.E., Duursma, R.A., Eamus, D., Ellsworth, D.S., Prentice, I.C., Barton, C.V.M.,
939 Crous, K.Y., De Angelis, P., Freeman, M., Wingate, L., 2011. Reconciling the optimal and
940 empirical approaches to modelling stomatal conductance. Glob. Change Biol. 17, 2134–2144.
941
942 Medvigy, D. M., S. C. Wofsy, J. W. Munger, D. Y. Hollinger, and P. R. Moorcroft (2009),
943 Mechanistic scaling of ecosystem function and dynamics in space and time: Ecosystem
944 Demography model version 2. J. Geophys. Res., 114, G01002.
945
946 Meinzer, F.C., 1993. Stomatal control of transpiration. Trends Ecol. Amp Evol., 8, 289–294.
947
948 Meinzer, F., Andrade, J., Goldstein, G., Holbrook, N., Cavelier, J., Jackson, P., 1997. Control
949 of transpiration from the upper canopy of a tropical forest: the role of stomatal, boundary
950 layer and hydraulic architecture components. Plant Cell Environ. 20, 1242–1252.
951

952 Miralles, D., De Jeu, R., Gash, J., Holmes, T., Dolman, A., 2011. Magnitude and variability
953 of land evaporation and its components at the global scale. Hydrol. Earth Syst. Sci., 15, 967-
954 981.

955

956 Miralles, D., van den Berg, M., Gash, J., Parinussa, R., de Jeu, R., Beck, H., Holmes, D.,
957 Jimenez, C., Verhoest, N., Dorigo, W., Teuling, A. J. and Dolman, J. 2014. El Niño–La Niña
958 cycle and recent trends in continental evaporation. Nature Clim. Change 4, 122–126

959

960 Mott, K., Parkhurst, D., 1991. Stomatal responses to humidity in air and helox. Plant Cell
961 Environ. 14, 509–515.

962

963 Mueller, B., Hirschi, M., Jimenez, C., Ciais, P., Dirmeyer, P., Dolman, A., Fisher, J., Jung,
964 M., Ludwig, F., Maignan, F., others, 2013. Benchmark products for land evapotranspiration:
965 LandFlux-EVAL multi-data set synthesis. Hydrol. Earth Syst. Sci. 17, 3707–3720.

966

967 Oleson, K.W., Lawrence, D.M., Bonan, G.B., Drewniak, B., Huang, M., Koven, C.D., Levis,
968 S., Li, F., Riley, W.J., Subin, Z.M., Swenson, S.C., Thornton, P.E., Bozbiyik, A., Fisher, R.,
969 Heald, C.L., Kluzek, E., Lamarque, J.-F., Lawrence, P.J., Leung, L.R., Lipscomb, W.,
970 Muszala, S., Ricciuto, D.M., Sacks, W., Sun, Y., Tang, J., Yang, Z.-L., 2013. Technical
971 Description of version 4.5 of the Community Land Model (CLM) (NCAR Technical Note No.
972 NCAR/TN-503+STR). Citeseer, National Center for Atmospheric Research, P.O. Box 3000,
973 Boulder, Colarado.

974

975 Pitman, A., 2003. The evolution of, and revolution in, land surface schemes designed for
976 climate models. Int. J. Clim. 23, 479–510.

977

978 Pitman, A.J., Avila, F.B., Abramowitz, G., Wang, Y.-P., Phipps, S.J., de Noblet-Ducoudré, N.
979 2011, Importance of background climate in determining impact of land-cover change on
980 regional climate. Nature Clim. Change, 1, 472–475.

981

982 Pollard, D., Thompson, S.L., 1995. Use of a land-surface-transfer scheme (LSX) in a global
983 climate model: the response to doubling stomatal resistance. Glob. Planet. Change 10, 129–
984 161.

985

986 Prentice, I. C., Dong, N. Gleason, S. M., Maire, V., Wright, I. J. 2014, Balancing the costs of
987 carbon gain and water transport: testing a new theoretical framework for plant functional
988 ecology. Ecology Letters, 17, 82-91.

989

990

991 Raupach, M., 1994. Simplified expressions for vegetation roughness length and zero-plane
992 displacement as functions of canopy height and area index. Bound.-Layer Meteorol. 71, 211–
993 216.

994

995 Raupach, M., Finkele, K., Zhang, L., 1997, SCAM (Soil-Canopy-Atmosphere Model):
996 Description and comparison with field data. Aspendale Aust. Csiro Cem Tech. Rep. 81.

997

998 Schymanski, S.J., Sivapalan, M., Roderick, M.L., Hutley, L.B., Beringer, J., 2009. An
999 optimality-based model of the dynamic feedbacks between natural vegetation and the water
1000 balance. Water Resour. Res. 45, W01412.

1001

1002 Schlaepfer, W., Ewers, D. R., Shuman, B.E. Williams, B. N, Frank, D. G., Massman, J. M.
1003 Lauenroth, W. J. 2014, Terrestrial water fluxes dominated by transpiration: Comment.
1004 Ecosphere 5.

1005

1006 Schlesinger, W.H., Jasechko, S. 2014, Transpiration in the global water cycle. Agric. For.
1007 Meteorol. 189, 115–117.

1008

1009 Sellers, P., Bounoua, L., Collatz, G., Randall, D., Dazlich, D., Los, S., Berry, J., Fung, I.,
1010 Tucker, C., Field, C., Jensen, T.G., 1996. Comparison of radiative and physiological effects of
1011 doubled atmospheric CO_2 on climate. Science 271, 1402–1406.

1012

1013 Sea, W. B., Choler, P., Beringer, J., Weinmann, R. A., Hutley, L. B., Leuning, R. 2011.
1014 Documenting improvement in leaf area index estimates from MODIS using hemispherical
1015 photos for Australian savannas. Agricultural and Forest Meteorology, 151, 1453–1461.

1016

1017 Serbin, S., Ahl, D. E., Gower, S. T. 2013, Spatial and temporal validation of the MODIS LAI
1018 and FPAR products across a boreal forest wildfire chronosequence. Remote Sens. Environ.,
1019 133, 71–84

1020

1021 Shabanov, N. V., Huang, D., Yang, W. Z., Tan, B., Knyazikhin, Y., Myneni, R. B., Ahl, D.
1022 E., Gower, S. T., Huete, A. R., Aragao, L.E.O.C., Shumabukuro, Y. E. 2005. Analysis and
1023 optimization of the MODIS leaf area index algorithm retrievals over broadleaf forests. IEEE
1024 Trans Geosci Remote Sens., 43, 1855–1865

1025

1026

1027 Stoy, P. C., Katul, G., Siqueira, M., Juang, J-Y., Novick, K. A., Uebelherr, J. M., Oren, R.
1028 2006. An evaluation of models for partitioning eddy covariance-measured net ecosystem
1029 exchange into photosynthesis and respiration. Agr. Forest Meteorol., 141, 2-18.

1030

1031 R Core Development Team, 2013. R: A Language and Environment for Statistical
1032 Computing. R Foundation for Statistical Computing, Vienna, Austria.

1033

1034 Wang, Y., Papanatsiou, M., Eisenach, C., Karnik, R., Williams, M., Hills, A., Lew, V.L.,
1035 Blatt, M.R., 2012. Systems Dynamic Modeling of a Guard Cell Cl− Channel Mutant
1036 Uncovers an Emergent Homeostatic Network Regulating Stomatal Transpiration. Plant
1037 Physiol. 160, 1956–1967.

1038

1039 Wang, Y.P., Kowalczyk, E., Leuning, R., Abramowitz, G., Raupach, M.R., Pak, B., van
1040 Gorsel, E., Luhar, A., 2011. Diagnosing errors in a land surface model (CABLE) in the time
1041 and frequency domains. J. Geophys. Res. Biogeosciences 2005–2012 116.

1042

1043 Wang, Y.P., Leuning, R., 1998. A two-leaf model for canopy conductance, photosynthesis
1044 and partitioning of available energy I: Model description and comparison with a multi-layered
1045 model. Agric. For. Meteorol. 91, 89–111.

1046

1047 Wullschleger, S.D., Meinzer, F., Vertessy, R., 1998. A review of whole-plant water use
1048 studies in tree. Tree Physiol. 18, 499–512.

1049

1050 Walden-Coleman, A.E., Rajcan, I., Earl, H.J., 2013. Dark-adapted leaf conductance, but not
1051 minimum leaf conductance, predicts water use efficiency of soybean (*Glycine max* L. Merr.).
1052 Can. J. Plant Sci., 93, 13–22.

1053

1054 Williams, M., Rastetter, E.B., Fernandes, D.N., Goulden, M.L., Wofsy, S.C., Shaver, G.R.
1055 and, 1996. Modelling the soil-plant-atmosphere continuum in a Quercus-Acer stand at
1056 Harvard Forest: the regulation of stomatal conductance by light, nitrogen and soil/plant
1057 hydraulic properties. Plant Cell Environ. 19, 911–927.

1058

1059 Zaehle, S., Friend, A., 2010. Carbon and nitrogen cycle dynamics in the O-CN land surface
1060 model: 1. Model description, site-scale evaluation, and sensitivity to parameter estimates.
1061 Glob. Biogeochem. Cycles 24, GB1005.

1062

1063 Zeppel, M. J. B., Lewis, J. D., Phillips, N., Tissue, D. T. (2014) Consequences of nocturnal
1064 water loss: a synthesis of implications for capacitance, embolism, and use in models. Tree
1065 Physiol., 34, 1047-1055.

1066

Zhang, Q., Pitman, A., Wang, Y., Dai, Y., Lawrence, P., 2013. The impact of nitrogen and phosphorous limitation on the estimated terrestrial carbon balance and warming of land use change over the last 156 yr. Earth Syst. Dyn. Discuss. 4, 507–539.

Zhou, S., Duursma, R.A., Medlyn, B.E., Kelly, J.W., Prentice, I.C., 2013. How should we model plant responses to drought? An analysis of stomatal and non-stomatal responses to water stress. Agric. For. Meteorol., 182-183, 204-214.

Zhou, S. Medlyn, B., Sabaté, S., Sperlich, D., Prentice, I. C. 2014, Short-term water stress impacts on stomatal, mesophyll and biochemical limitations to photosynthesis differ consistently among tree species from contrasting climates. Tree Physiol, 34, 1035-1046.

Figure Captions

Figure 1: Stomatal sensitivity to increased vapour pressure deficit (D). The Leuning model has been parameterised in the same way as the CABLE model, for C3 species: a_1 = 9.0, D = 1.5 kPa and for C4 plants: a_1 = 4.0, D_0 = 1.5 kPa. The Medlyn model has been fit to output generated by the Leuning model using least squares for D ranging from 0.05 to 3 kPa. The calibrated parameters for the Medlyn model were g_1 = 3.37 and g_1 = 1.09 for C3 and C4 species, respectively.

Figure 2: Map showing the plant functional types (PFTs) currently used in CABLE (Lawrence et al. 2012). CABLE also has C4 crop, wetland and urban PFTs, however these are currently not operational.

Figure 3: A comparison of the modelled average seasonal cycle of gross primary productivity (GPP), latent heat flux (LE), transpiration (E) and the observed (OBS) LE flux at 6 FLUXNET sites during approx. daylight hours (8 am – 7 pm). Timeseries have been averaged across all years as described in Table 4 to produce seasonal cycles. Light blue shading indicates the uncertainty in predicted fluxes from the Medlyn model (MED-P), accounting for ± 2 standard errors in the site g_1 parameter value.

Figure 4: Mean diurnal modelled gross primary productivity (GPP), latent heat flux (LE), transpiration (E) and the observed (OBS) LE flux at the Howard Springs Fluxnet sites during daylight hours (8 am – 7 pm). Timeseries have been averaged across all years as described in Table 2 to produce diurnal seasonal cycles. Light blue shading indicates the uncertainty in predicted fluxes from the Medlyn model (MED-P), accounting for ± 2 standard errors in the site g_1 parameter value.

Figure 5: Average seasonal cycles of the simulated decoupling coefficient (Ω), total boundary layer conductance (g_b) and stomatal conductance (g_s) at 6 Fluxnet sites during daylight hours (8 am – 7 pm). Timeseries have been averaged across all years as described in Table 2 to produce seasonal cycles. Light blue shading indicates the uncertainty in predicted fluxes from

1119 the Medlyn model (MED-P), accounting for ± 2 standard errors in the site g_1 parameter value.

1120

1121 Figure 6: Global maps showing how the g_1 model parameter varies across the globe. Panel (a)
1122 shows the fitted g_1 parameter values for each PFT based on the data, panel (b) shows the
1123 predicted g_1 parameter values considering the influence of climate indices. In total, 126 out of
1124 a possible 54,000 pixels have been masked from panel (b), representing pixels where the
1125 temperature range and moisture index extended outside the range of the database of Lin et al.
1126 (2015).

1127

1128 Figure 7: Mean seasonal (December-January-February: DJF and June-July-August: JJA)
1129 difference maps of gross primary productivity (GPP) calculated across the 10 years of the
1130 Global Soil Wetness Project2 (GSWP-2) forcing (1986-1995) period. Panels (a) and (b) show
1131 the difference between the standard CABLE (LEU) model and the Medlyn model fit to the
1132 Leuning model (MED-L), panels (c) and (d) show the difference between the LEU model and
1133 the Medlyn model with the g_1 PFT parameterisation (MED-P), and finally, panels (e) and (f)
1134 show the difference between the LEU model and the Medlyn model with the g_1 parameter
1135 predicted as a function of climate indices (MED-C). In total, 126 out of a possible 54,000
1136 pixels have been masked from panels (e) and (f), representing pixels where the temperature
1137 range and moisture index extended outside the range of the synthesis g_s database. ata shown
1138 in panels (b), (c), (d), (e), (f) have been clipped, with the maximum ranges extending to (-1.6–
1139 0.36), (-1.28–3.03), (-1.19–3.82), (-1.2–2.9) and (-1.05–3.7) and this affects 1, 64, 34, 42 and
1140 147 pixels, respectively.

1141

1142 Figure 8: Mean seasonal (December-January-February: DJF and June-July-August: JJA)
1143 difference maps of transpiration (E) calculated across the 10 years of the Global Soil Wetness
1144 Project2 (GSWP-2) forcing (1986-1995) period. Panels (a) and (b) show the difference
1145 between the standard CABLE (LEU) model and the Medlyn model fit to the Leuning model
1146 (MED-L), panels (c) and (d) show the difference between the LEU model and the Medlyn
1147 model with the g_1 PFT parameterisation (MED-P), and finally, panels (e) and (f) show the
1148 difference between the LEU model and the Medlyn model with the g_1 parameter predicted as

a function of climate indices (MED-C). In total, 126 out of a possible 54,000 pixels have been masked from panels (e) and (f), representing pixels where the temperature range and moisture index extended outside the range of the synthesis g_s database. Data shown in panels (c), (d), (e), (f) have been clipped, with the maximum ranges extending to (-0.3–1.12), (-0.33–1.27), (-0.63–0.84) and (-0.64–1.31) and this affects 36, 251, 8 and 444 pixels, respectively.

Figure 9: Latitudinal average (December-January-February: DJF and June-July-August: JJA) of mean annual (a,b) gross primary productivity (GPP) and (c,d) evapotranspiration (ET) predicted by the CABLE model compared to the upscaled FLUXNET and LandFlux-EVAL products. CABLE model simulations are shown are from the standard CABLE (LEU), the Medlyn model fit to the Leuning model (MED-L), Medlyn model with the g_1 PFT parameterisation (MED-P) and the Medlyn model with the g_1 parameter predicted as a function of climate indices (MED-C). The shading represents ± 1 standard deviation in the data product and ± 2 standard errors in the MED-P and MED-C models. Data shown cover the 10 years of the Global Soil Wetness Project2 (GSWP-2) forcing (1986-1995) period. In total, 126 out of a possible 54,000 pixels have been masked from the zonal average of the MED-C model, which represents pixels where the temperature range and moisture index extended outside the range of the synthesis g_s database. Missing data areas in the both data products have been also been excluded from any comparisons (for example over the Sahara Desert, see Zhang et al. 2013).

Figure S1: Global maps showing the uncertainty of the g_1 model parameter. Panel (a) shows –2 standard errors (SE) and (b) + 2 SE for the fitted g_1 for each of CABLE's PFTs. Panel (c) shows –2 standard errors (SE) and (e) + 2 SE for predicted g_1 parameter values considering the influence of climate indices. In total, 126 out of a possible 54,000 pixels have been masked from panels (c) and (d), representing pixels where the temperature range and moisture index extended outside the range of the synthesis g_s database.

Figure S2: Minimum measured stomatal conductance (g_s) as a function of corresponding photosynthesis rate, for each dataset in the Lin et al. (2015) synthesis g_s database with minimum photosynthesis rate < 5 mol m^{-2} s^{-1}. Data are separated into C3 (131 datasets) and

1180 C4 species (22 datasets). Also shown for comparison are the default g_0 values used in
1181 CABLE, as well as average night-time g_0 values for C3 and C4 plants, calculated from Figure
1182 2 in a review by Zeppel et al. (2014).

1183
1184

1185 Tables

1186 Table 1: Fitted g_1 values based on the CABLE PFTs using data from Lin et al. (2015).

PFT	g_1 mean ($kPa^{0.5}$)	g_1 standard error ($kPa^{0.5}$)
Evergreen needleleaf	2.35	0.25
Evergreen broadleaf	4.12	0.09
Deciduous needleleaf	2.35	0.25
Deciduous broadleaf	4.45	0.36
Shrub	4.70	0.82
C3 grassland	5.25	0.32
C4 grassland	1.62	0.13
Tundra	2.22	0.4
C3 cropland	5.79	0.64

1187

1188 Table 2: Model coefficients used in mixed effects model to predict g_1 from two long-term
1189 average (1960-1990) bioclimatic variables: temperature and a moisture index representing an
1190 indirect estimate of plant water availability.

PFT	*a*	*b*	*c*	*d*	*e*
Evergreen needleleaf	1.32	0.03	0.02	0.01	-0.97
Evergreen broadleaf	1.32	0.03	0.02	0.01	-0.67
Deciduous needleleaf	1.32	0.03	0.02	0.01	-0.97
Deciduous broadleaf	1.32	0.03	0.02	0.01	-0.37
Shrub	1.32	0.03	0.02	0.01	-0.29
C3 grassland	1.32	0.03	0.02	0.01	-0.1
C4 grassland	1.32	0.03	0.02	0.01	-1.35
Tundra	1.32	0.03	0.02	0.01	-0.73

C3 cropland	1.32	0.03	0.02	0.01	0.0

Table 3: A summary of model simulations

Model Simulation	Description
LEU	Control experiment, standard CABLE model with the Leuning g_s model.
MED-L	Medlyn model with parameters (g_0 and g_1) calibrated against an offline Leuning model.
MED-P	Medlyn model with the g_1 parameter calibrated by PFT constrained by a global synthesis of stomatal data.
MED-C	Medlyn model with the g_1 parameters predicted from a mixed effects model considering the impacts of temperature and aridity.

Table 4: Summary of flux tower sites.

Site	FLUXNET Vegetation Type	CABLE PFT	Latitude	Longitude	Country	Years	Reference
Bondville	Cropland	C3 Crop	40.00 N	-88.29 W	US	1997-2006	
Cabauw	Grassland	C3 Grass	51.97 N	4.93 E	Holland	2003-2006	
Harvard	Deciduous broadleaf	Deciduous broadleaf	42.54 N	-72.17 W	US	1994-2001	
Howard Springs	Woody Savannah	C4 grass	-12.49 S	131.15 E	Australia	2002-2005	

Hyytiala	Evergreen needleleaf	Evergreen needleleaf	61.85 N	23.29 E	Finland	2001-2004
Tumbarumba	Evergreen broadleaf	Evergreen broadleaf	-35.66 S	148.15 E	Australia	2002-2005

1196

1197 Table 5: Summary statistics of modelled and observed LE at the 6 FLUXNET sites during
1198 daylight hours (9 am – 18 pm) and over the peak-growing season (for Northern hemisphere
1199 sites, from June–July–August and for Southern Hemisphere sites, from December–January–
1200 February).

Site	RMSE			Bias			Index of Agreement		
	LEU	MED-L	MED-P	LEU	MED-L	MED-P	LEU	MED-L	MED-P
Bondville	109.91	102.74	109.78	-12.92	-9.50	-5.80	0.81	0.83	0.84
Cabauw	82.13	78.65	82.76	-13.54	-13.15	-12.75	0.78	0.80	0.79
Harvard	59.17	55.51	58.51	8.35	4.10	7.10	0.94	0.95	0.95
Howard Springs	105.92	105.72	138.57	-4.86	1.16	-61.25	0.83	0.84	0.62
Hyytiala	58.90	54.62	47.33	21.00	16.26	-0.24	0.89	0.89	0.89
Tumbarumba	130.91	124.28	124.84	-15.06	-14.30	-13.22	0.76	0.78	0.78

1201

1202 Table 6: Mean and 1 standard deviation difference in annual GPP between the LEU and
1203 MED-L model, the LEU and MED-P models and the LEU-C models for each of CABLE's
1204 PFTs. Where standard deviations are large relative to the mean it suggests large variability
1205 between the LEU and other models within a PFT.

PFT	GPP: LEU − MED-L ($g\ C\ m^{-2}\ y^{-1}$)	GPP: LEU − MED-P ($g\ C\ m^{-2}\ y^{-1}$)	GPP: LEU − MED-C ($g\ C\ m^{-2}\ y^{-1}$)
Evergreen needleleaf	-3.08 ± 18.39	39.05 ± 34.18	43.45 ± 24.2
Evergreen broadleaf	36.1 ± 51.93	76.12 ± 61.99	73.70 ± 65.08
Deciduous needleleaf	-1.84 ± 5.14	24.06 ± 5.35	34.03 ± 5.75
Deciduous broadleaf	-31.48 ± 57.77	-17.31 ± 38.0	-46.3 ± 69.01

Shrub	-69.28 ± 32.31	-45.46 ± 17.61	-35.39 ± 17.41
C3 grassland	-47.73 ± 46.83	-66.76 ± 41.55	-62.79 ± 50.02
C4 grassland	-93.04 ± 45.95	302.94 ± 113.93	115.53 ± 89.29
Tundra	0.3 ± 12.63	16.61 ± 14.16	13.36 ± 11.02
C3 cropland	-26.85 ± 36.51	-64.93 ± 36.58	-65.45 ± 58.21

1206

1207 Table 7: Mean and 1 standard deviation difference in annual E between the LEU and MED-L
1208 model, the LEU and MED-P models and the LEU-C models for each of CABLE's PFTs.
1209 Where standard deviations are large relative to the mean it suggests large variability between
1210 the LEU and other models within a PFT.

PFT	E: LEU − MED-L ($mm\ y^{-1}$)	E: LEU − MED-P ($mm\ y^{-1}$)	E: LEU − MED-C ($mm\ y^{-1}$)
Evergreen needleleaf	16.55 ± 9.78	76.27 ± 36.34	81.72 ± 29.36
Evergreen broadleaf	34.34 ± 14.34	27.31 ± 14.7	22.66 ± 48.16
Deciduous needleleaf	10.5 ± 6.18	54.36 ± 17.07	67.03 ± 17.83
Deciduous broadleaf	11.15 ± 13.61	0.56 ± 8.45	-10.16 ± 34.36
Shrub	-11.14 ± 5.2	-4.81 ± 5.51	-1.68 ± 6.21
C3 grassland	0.34 ± 10.68	-17.37 ± 8.63	-15.51 ± 19.63
C4 grassland	-11.99 ± 5.67	107.77 ± 41.88	47.34 ± 32.21
Tundra	5.9 ± 3.87	24.13 ± 14.38	20.96 ± 11.75
C3 cropland	0.8 ± 12.37	-30.07 ± 12.36	-28.56 ± 30.11

1211

1212 Table 8: Summary statistics for December–January–February (DJF) June–July–August (JJA),
1213 describing the root mean squared error (RMSE) and bias between the FLUXNET-MTE GPP
1214 product and the CABLE model.

PFT	LEU (JJA; DJF)	MED-P (JJA; DJF)	MED-C (JJA; DJF)

	RMSE	Bias	RMSE	Bias	RMSE	Bias
Evergreen needleleaf	3.23; 0.4	2.73; 0.11	2.98; 0.39	2.42; 0.1	2.92; 0.39	2.37; 0.1
Evergreen broadleaf	2.31; 2.29	1.87; 1.57	2.14; 2.16	1.66; 1.36	2.12; 2.09	1.68; 1.36
Deciduous needleleaf	4.41; 0.00	4.37; 0.00	4.17; 0.00	4.13; 0.00	4.07; 0.00	4.03; 0.00
Deciduous broadleaf	2.33; 1.81	1.75; 1.27	2.33; 1.88	1.78; 1.33	2.35; 1.97	1.82; 1.42
Shrub	0.98; 0.86	0.72; 0.51	1.10; 0.95	0.84; 0.61	1.08; 0.91	0.82; 0.57
C3 grassland	1.86; 1.44	1.37; 0.85	2.09; 1.57	1.67; 0.97	2.06; 1.59	1.61; 0.99
C4 grassland	3.15; 2.36	2.55; 1.73	2.43; 1.67	1.77; 0.94	2.94; 2.16	2.24; 1.43
Tundra	2.48; 0.29	1.79; 0.03	2.31; 0.27	1.62; 0.03	2.34; 0.27	1.66; 0.03
C3 cropland	1.96; 1.25	1.33; 0.83	2.18; 1.39	1.64; 0.94	2.13; 1.43	1.59; 0.96

Table 9: Summary statistics for December–January–February (DJF) June–July–August (JJA), describing the root mean squared error (RMSE) and bias taking the GLEAM ET product as reference.

PFT	LEU (JJA; DJF)		MED-P (JJA; DJF)		MED-C (JJA; DJF)	
	RMSE	Bias	RMSE	Bias	RMSE	Bias
Evergreen	2.37; 1.83	0.79; 0.24	2.28; 1.83	0.31; 0.23	2.27; 1.83	0.26; 0.23

needleleaf						
Evergreen broadleaf	2.17; 2.32	-0.05; -0.25	2.18; 2.34	-0.12; -0.32	2.17; 2.32	-0.1; -0.31
Deciduous needleleaf	1.45; 0.69	1.15; -0.02	1.19; 0.69	0.75; -0.02	1.13; 0.69	0.65; -0.0
Deciduous broadleaf	2.69; 2.43	0.79; 0.58	2.69; 2.43	0.77; 0.58	2.69; 2.43	0.78; 0.61
Shrub	1.25; 1.34	0.29; 0.47	1.24; 1.34	0.29; 0.46	1.25; 1.34	0.29; 0.45
C3 grassland	1.66; 1.49	0.53; 0.34	1.67; 1.5	0.55; 0.36	1.67; 1.5	0.54; 0.37
C4 grassland	1.37; 1.38	0.33; 0.29	1.32; 1.35	0.2; 0.09	1.35; 1.35	0.29; 0.2
Tundra	2.35; 1.88	0.74; 0.37	2.31; 1.88	0.55; 0.36	2.31; 1.88	0.57; 0.36
C3 cropland	1.8; 1.38	0.9; 0.29	1.85; 1.39	0.98; 0.3	1.84; 1.39	0.97; 0.3

1221

1222

Figure 1

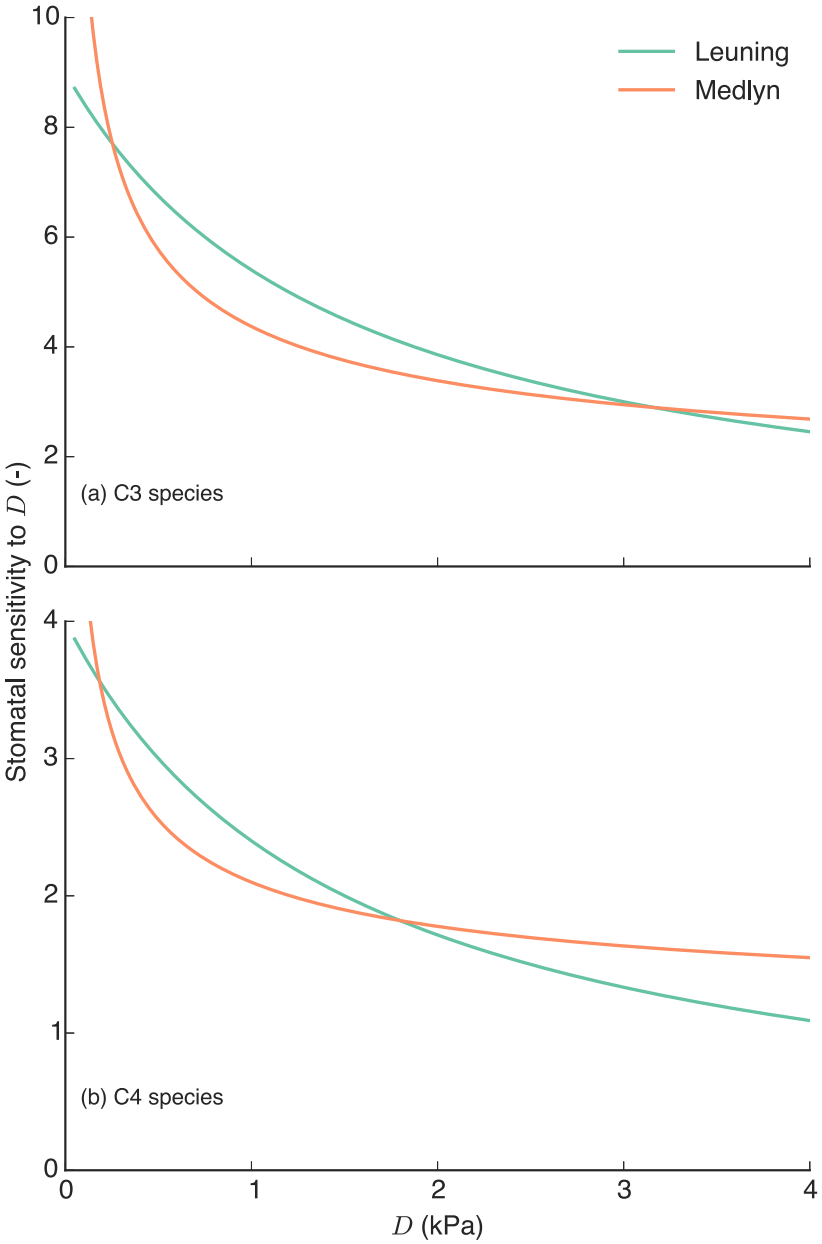
Leuning
Medlyn
(a) C3 species
(b) C4 species
Stomatal sensitivity to D (-)
D (kPa)
0
2
4
6
8
10
1
3

Figure 2

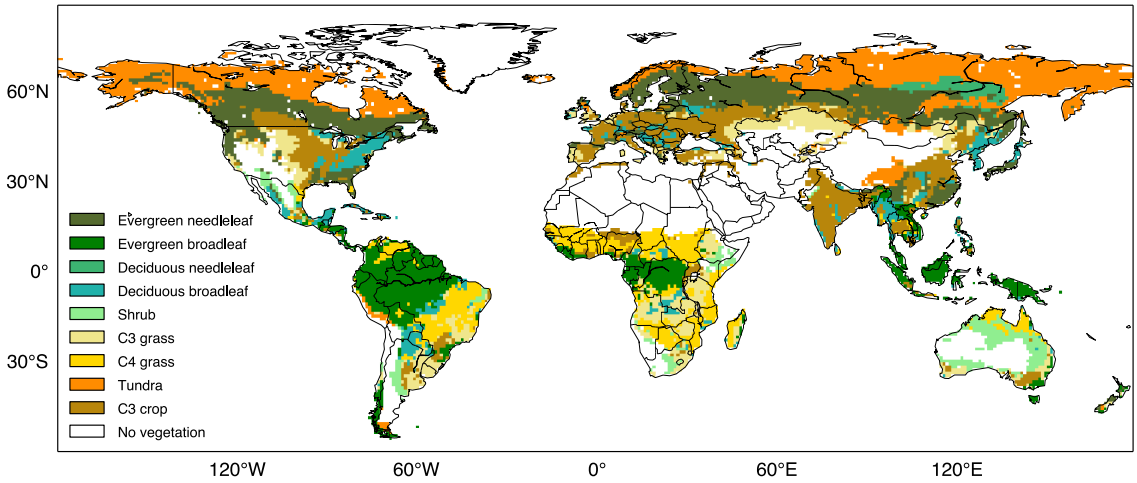
60°N
30°N
0°
30°S
Evergreen needleleaf
Evergreen broadleaf
Deciduous needleleaf
Deciduous broadleaf
Shrub
C3 grass
C4 grass
Tundra
C3 crop
No vegetation
120°W
60°W
0°
60°E
120°E

Figure 3

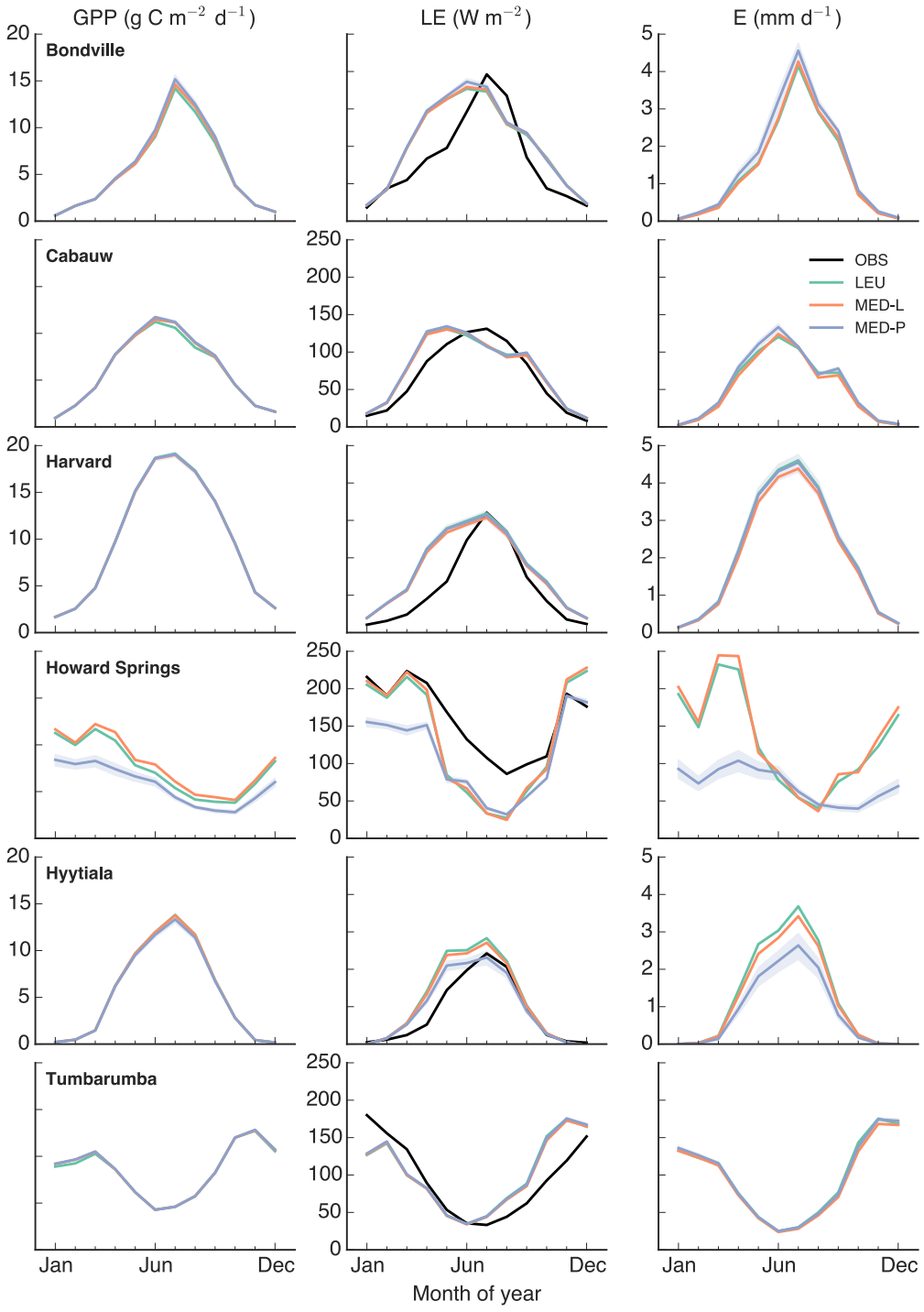
GPP (g C m^{-2} d^{-1})
LE (W m^{-2})
E (mm d^{-1})
Bondville
Cabauw
Harvard
Howard Springs
Hyytiala
Tumbarumba
OBS
LEU
MED-L
MED-P
Jan
Jun
Dec
Month of year

Figure 4

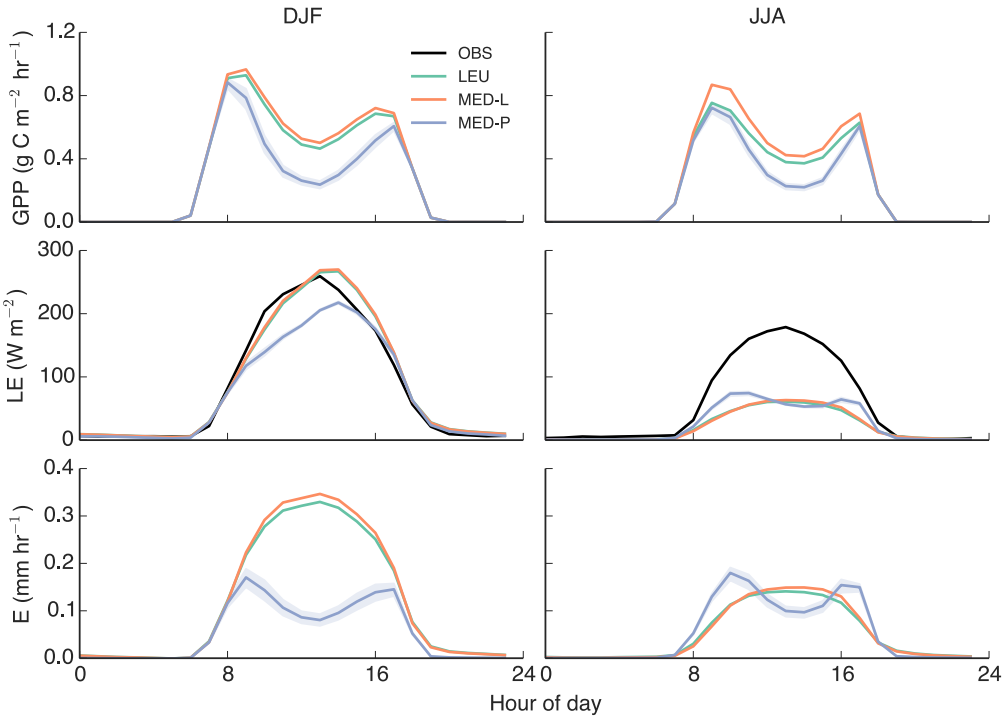
DJF
JJA
OBS
LEU
MED-L
MED-P
GPP (g C m^{-2} hr^{-1})
LE (W m^{-2})
E (mm hr^{-1})
1.2
0.8
0.4
0.0
300
200
100
0
0.4
0.3
0.2
0.1
0.0
0
8
16
24
Hour of day

Figure 5

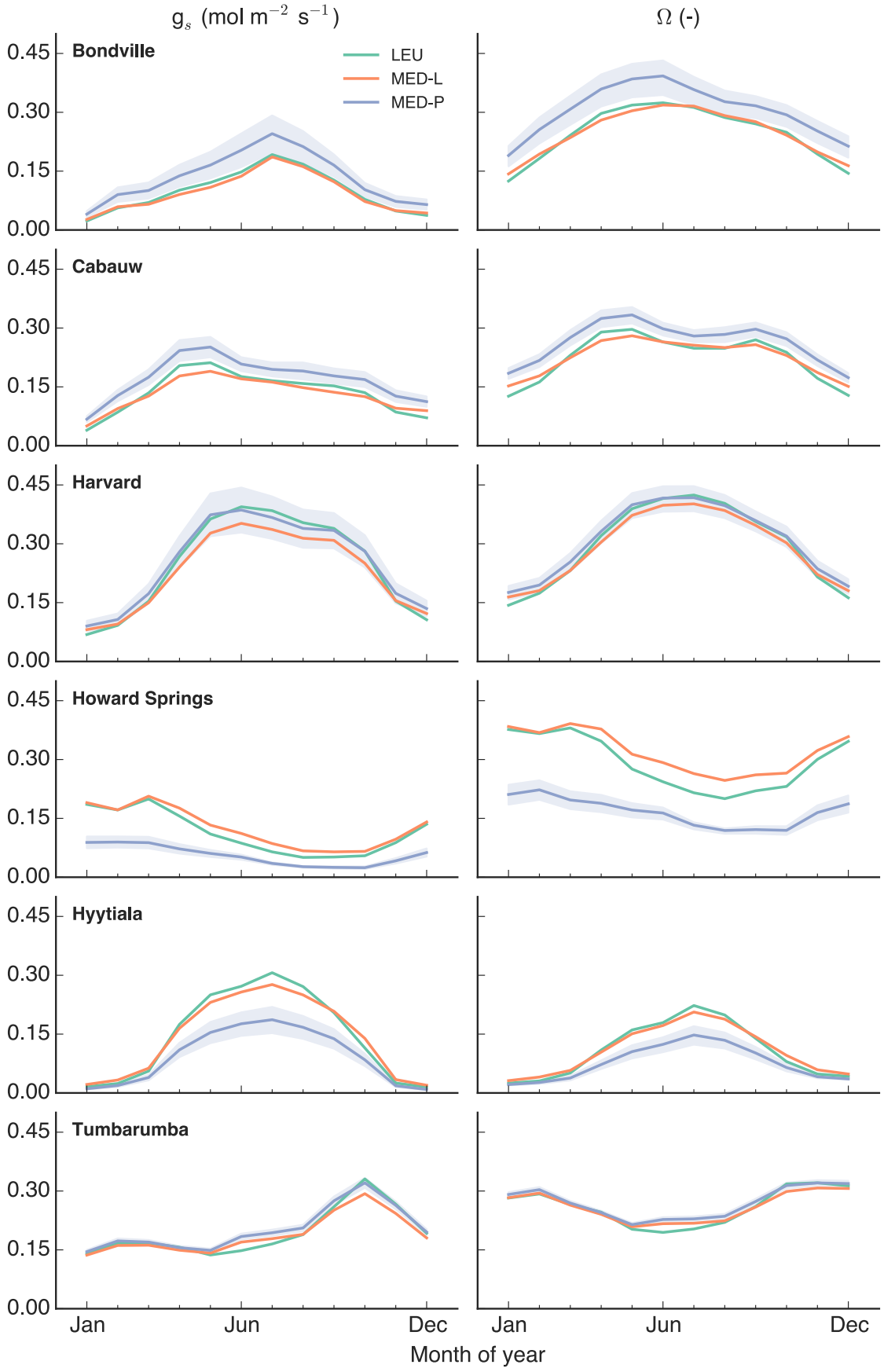
g_s (mol m^{-2} s^{-1})
Ω (-)
LEU
MED-L
MED-P
Bondville
Cabauw
Harvard
Howard Springs
Hyytiala
Tumbarumba
0.45
0.30
0.15
0.00
Jan
Jun
Dec
Month of year

Figure 6

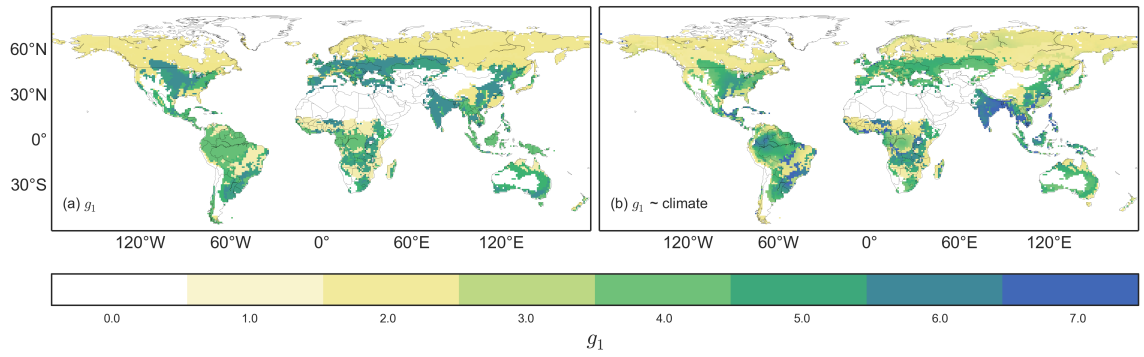
60°N
30°N
0°
30°S
(a) g_1
(b) g_1 ~ climate
120°W
60°W
0°
60°E
120°E
0.0
1.0
2.0
3.0
4.0
5.0
6.0
7.0
g_1

Figure 7

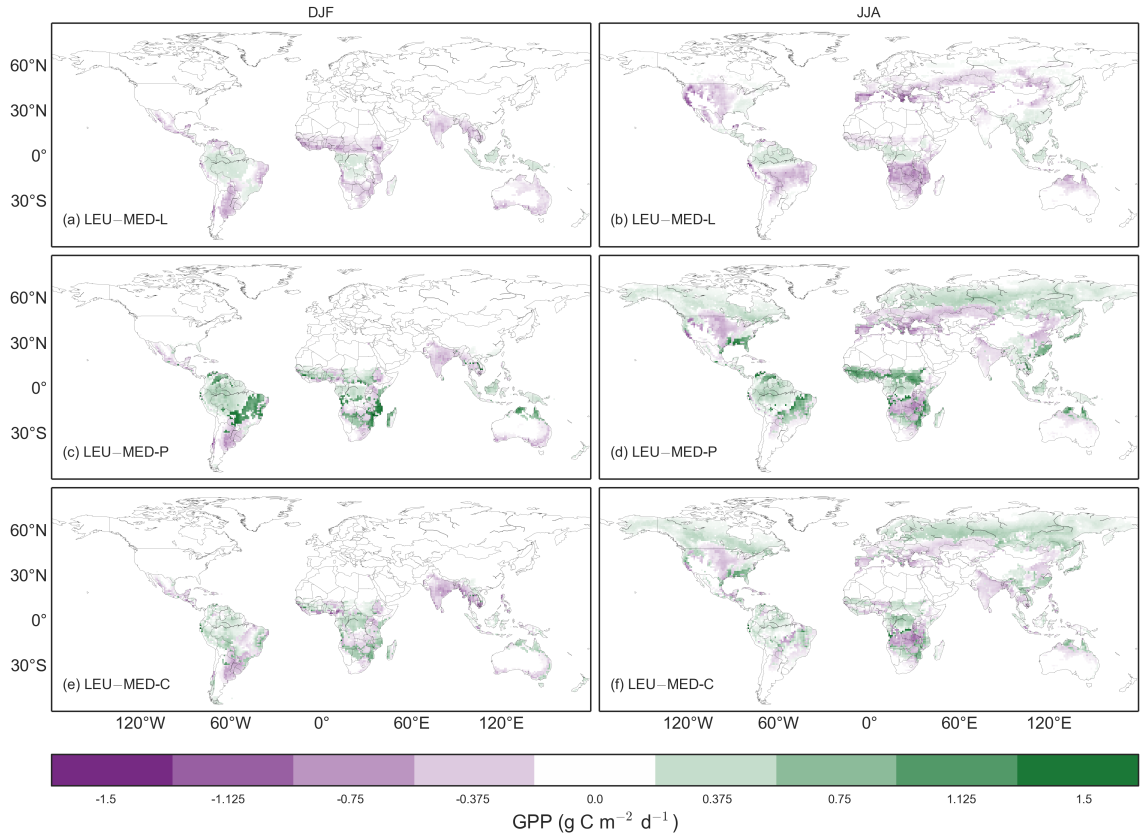
DJF
JJA
60°N
30°N
0°
30°S
(a) LEU−MED-L
(b) LEU−MED-L
(c) LEU−MED-P
(d) LEU−MED-P
(e) LEU−MED-C
(f) LEU−MED-C
120°W
60°W
0°
60°E
120°E
-1.5
-1.125
-0.75
-0.375
0.0
0.375
0.75
1.125
1.5
GPP (g C m^{-2} d^{-1})

Figure 8

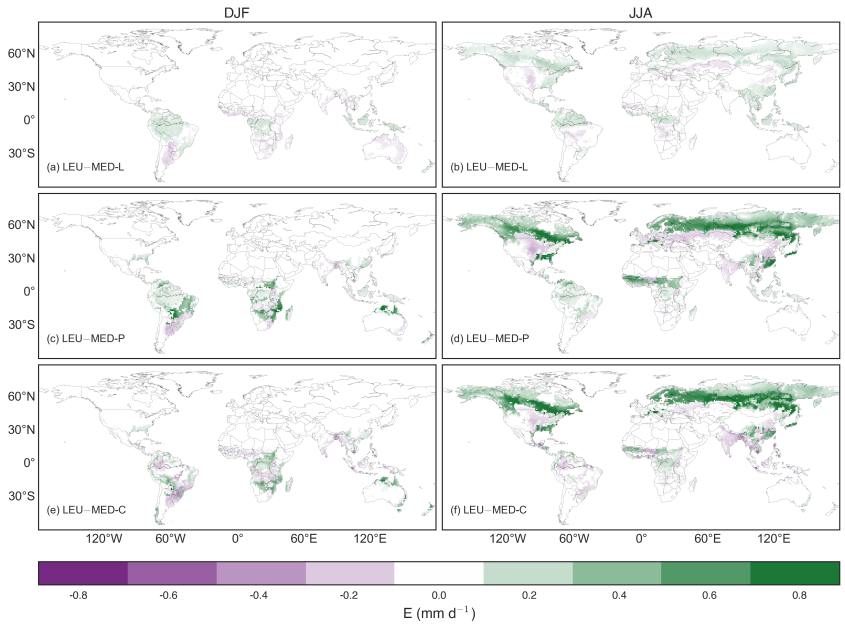
DJF
JJA
60°N
30°N
0°
30°S
(a) LEU−MED-L
(b) LEU−MED-L
(c) LEU−MED-P
(d) LEU−MED-P
(e) LEU−MED-C
(f) LEU−MED-C
120°W
60°W
0°
60°E
120°E
-0.8
-0.6
-0.4
-0.2
0.0
0.2
0.4
0.6
0.8
E (mm d⁻¹)

Figure 8

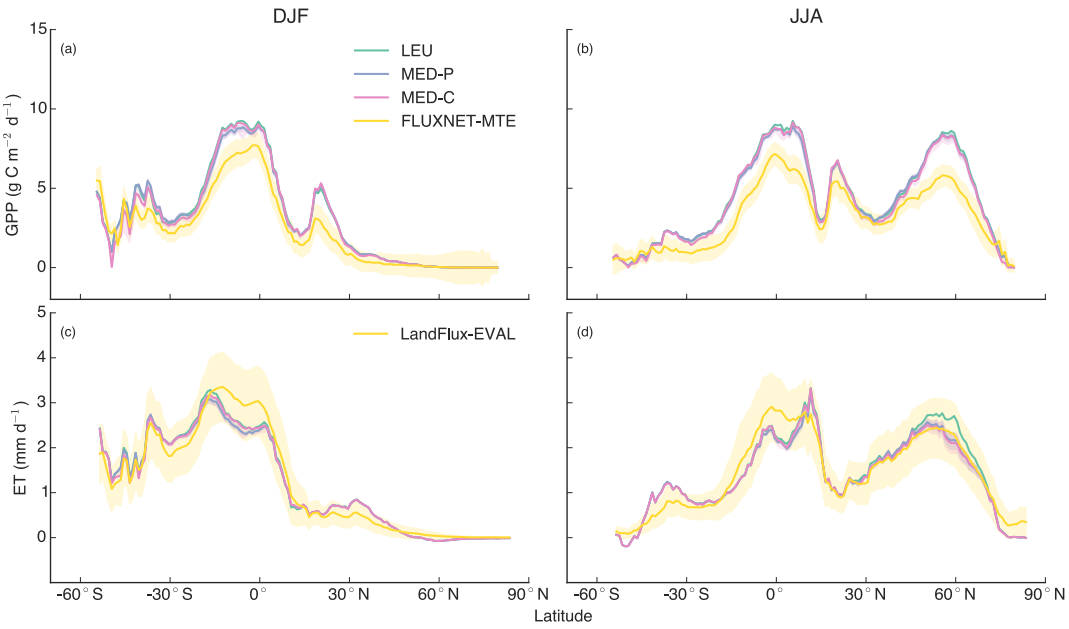
DJF
JJA
(a)
(b)
(c)
(d)
LEU
MED-P
MED-C
FLUXNET-MTE
LandFlux-EVAL
GPP (g C m^{-2} d^{-1})
ET (mm d^{-1})
-60° S
-30° S
0°
30° N
60° N
90° N
Latitude

Figure S1

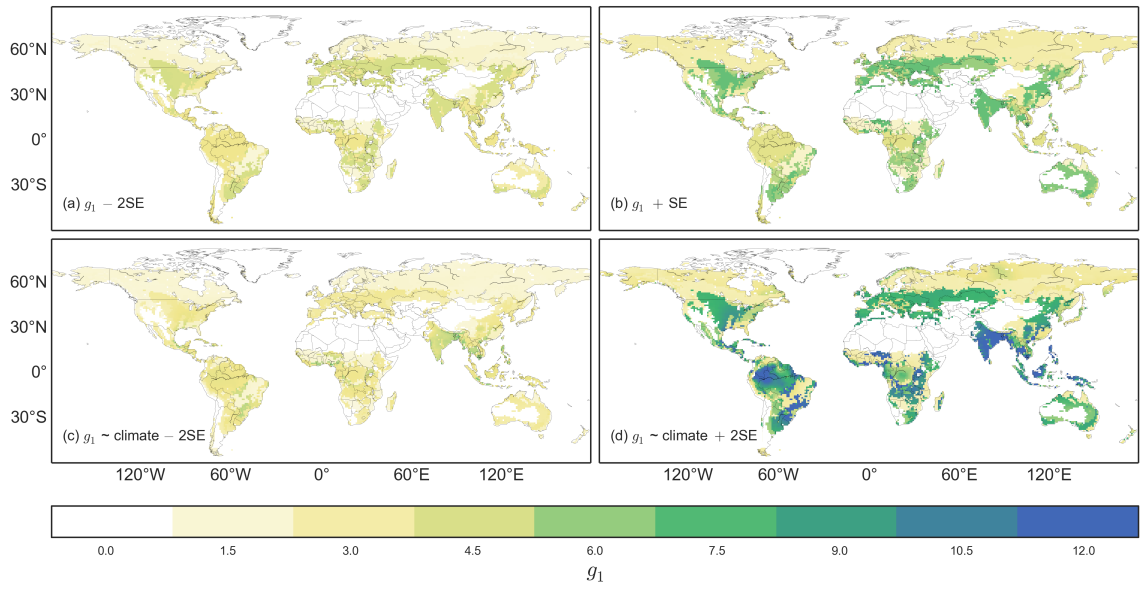
60°N
30°N
0°
30°S
(a) g_1 − 2SE
(b) g_1 + SE
(c) g_1 ~ climate − 2SE
(d) g_1 ~ climate + 2SE
120°W
60°W
0°
60°E
120°E
0.0
1.5
3.0
4.5
6.0
7.5
9.0
10.5
12.0
g_1

Figure S2

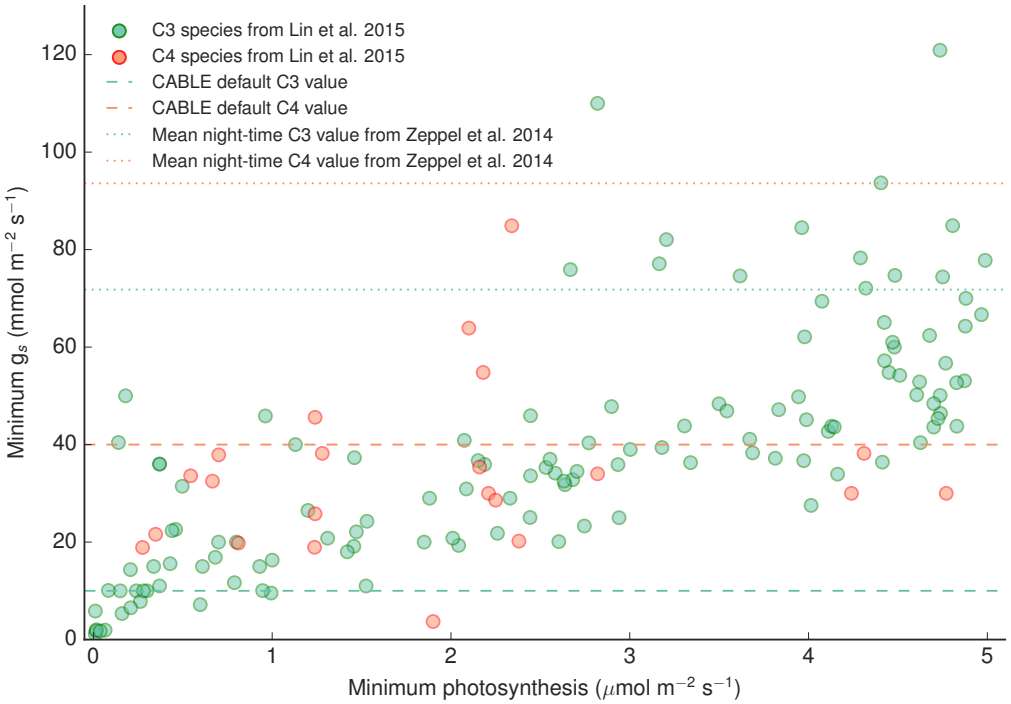
C3 species from Lin et al. 2015
C4 species from Lin et al. 2015
CABLE default C3 value
CABLE default C4 value
Mean night-time C3 value from Zeppel et al. 2014
Mean night-time C4 value from Zeppel et al. 2014
Minimum g_s (mmol m^{-2} s^{-1})
Minimum photosynthesis (μmol m^{-2} s^{-1})
0
20
40
60
80
100
120
0
1
2
3
4
5